December 2011

Investigations on Detector Non-Linear Response for the Optimization of Laser-Induced Phosphorescence Decay-Time Detection.

Fahed Abou Nada,

Division of Combustion Physics
Lund University

60 ECTS

MASTER OF SCIENCE THESIS

Mattias Richter
Christoph Knappe

December 19, 2011
Lund Reports on Combustion Physics, LRCP-148
ISRN LUTFD2/TFC--148--SE
ISSN 1102-8718

Fahed Abou Nada
Division of Combustion Physics
Lund University
P.O. Box 118
S-221 00 Lund
Sweden

Dedicated to my Mother and Father for their Love, Endless support, and Encouragement

Abstract

This thesis investigates the nonlinear detector response to Laser Induced Phosphorescence signal originating from the $CdWO_4$ phosphor. A matrix method is utilized to map the detectors linearity for decay-time determination as function of detector gain and number of photons reaching the detector. The Matrix is created by scanning the energy of the laser beam hitting the phosphor thus changing the phosphorescence intensity while fixing the detector at constant gain. Then detector gain is changed and the same process repeated for the full gain range chosen for each detector. Four different detectors are used in the experiment; some of them have the capability to be run in time-gated mode. The detectors used are photomultiplier tube, time-gated photomultiplier tube, micro-channel plate photomultiplier tube, and avalanche photodiode. The experiment was conducted at five temperatures in between 21 and 290 °C and cover the full decay-time range of the $CdWO_4$ (5ns-15μs). The detector nonlinearity changes the computed decay-time of the phosphorescence, leading to error in the temperature found. Nonlinearity can originate from two saturation effects. The first is optical saturation that is due to the saturation of the detector photocathode under increasing radiation intensity, whereas the second is electrical saturation that is due to saturation in the electron multiplication mechanism. Using the matrix of detector response nonlinear detector operating regions can be found for any detector and actions can be undertaken to correct or avoid saturated signals.

Abstrakt

Detta Masters-arbete beskriver resultaten från undersökningar av den icke-lineära responsen hos fotomultiplikatorer då dessa detekterar signalen från den termografiska fosforn $CdWO_4$ som är vanligt förekommande vid fosforbaserade temperaturmätningar. En matrismetod har använts för att kartlägga detektorns linearitet i samband med livstidsmätningar, som funktion av förstärkningsnivå och antal fotoner per tidsenhet som når detektorn. Variationerna i matrisen skapas genom att den laserenergi som träffar fosforprovet sveps, vilket varierar fosforescensintensiteten som når detektorn, medan fotomultiplikatorns förstärkningsnivå hålles konstant. Sedan ändras förstärkningen successivt samtidigt som laserenergisvepet upprepas för varje förstärkningsnivå tills hela förstärkningsområdet undersökts.
Fyra olika typer av fotomultiplikatorer har studerats; konventionell fotomultiplikator, ”time-gated” fotomultiplikator, micro-channel plate (MCP) fotomultiplikator samt ”avalanche” fotodiod. Den experimentella studien omfattar mätningar vid fem olika temperaturer mellan 21 och 290 °C, och täcker därmed hela spannet av livstider från fosforn $CdWO_4$ (5ns-15µs). Icke-lineartiteter hos detektorns intensitetsrespons påverkar analysen av fosforns livstid vilket i förlängningen medför ett fel när temperaturen beräknas. Icke-lineariteten kan anses vara orsakad av två huvudsakliga mättnadseffekter. Den första kan tillskrivas optisk mättnad och uppstår när fotokatoden mättas av för många inkommande fotoner per tidsenhet. Den andra typen, elektrisk mättnad, uppstår i elektronmultiplikatorkedjan. Genom att tillämpa den föreslagna matrismetoden kan icke-lineära arbetsområden identifieras för flertalet typer av optiska detektorer. I rapporten föreslås också en metod för hur denna oönskade mättnadseffekt kan undvikas, alternativt kompenseras för.

Acknowledgements

I would like to express my gratitude to my supervisors, PhD candidate Christoph Knappe and Prof. Mattias Richter, who gave the chance to complete my thesis and for their help and support during a period of one year. I would like also to thank the Head of the Combustion Department Prof. Marcus Aldén and the staff at the Combustion Physics department for their help and support. My greatest appreciation to Lennart Osterman for his help in building and modifying electric circuits for the detectors.

I would like to thank all of my family and friends for their patience and support during my Masters study at Lund University. Special thanks to my friend and project partner Nawzad Al-Habib as we worked together for the first six months of my thesis discussing problems and working together in the laboratory.

This page has been intentionally left blank.

1. Introduction

Laser Induced Phosphorescence (LIP) is a temperature measuring technique that relies on the temperature dependence of the decay-time of the thermographic phosphor. The phosphor is excited by laser radiation and the phosphorescence decay time is measured using a photoelectric detector that converts photon in to electrons. Usually the detector used is a photomultiplier tube (PMT) due to its advantages such as fast response, low noise level, and high gain compared to other detectors. However, using the photomultiplier or any other photoelectric detector under intense light conditions and very high gain causes the detector to deviate from normal operation. This deviation is due to saturation of the detector that can be sub-categorized into electrical saturation and optical saturation. The optical saturation is due to electron depletion that occurs at the photocathode. Electrical saturation is resulted from the nonlinear response in the amplification process in the detector that is governed by the secondary electron emission. For example, electric saturation occurs when at least one dynode in the amplification chain fails to reproduce proportional an amount of electrons due to accumulation of space charges. The optical saturation is due to electron depletion that occurs at the photocathode. The photocathode function is to convert the photons hitting its surface into electrons that accelerates under an applied potential towards the secondary electron amplification stage.

These saturation effects result in variation of the evaluated phosphorescence decay-time and by succession in a variation of the temperature calculated. The degree of variation depends on the conditions applied during the operation of the photoelectric detector. The aim of this thesis is to characterize four detectors as a function of phosphorescence intensity and gain by investigating the detected decay time. Measurement results are mapped into a detector specific response matrix containing averaged decay times in each matrix element. Areas of constant decay time describe desirable operation conditions showing that the detector is unsusceptible to minor changes in gain or intensity. This procedure is repeated at five different temperatures to achieve a library of the detector for the whole response range of the phosphor. The detectors used are varying from normal photomultiplier tube (PMT), avalanche photodiode (APD), micro-channel plate photomultiplier tube (MCP-PMT), to time-gated photomultiplier tube. A comparison is built upon the response of each detector compared to the other and to different modes of operation. For example, a single detector might have the option to be run in continuous or time gated mode. A detector specific matrix library can be built for any detector with the gain and light intensity ranges that best suit the experimental conditions for a given phosphor.

2. Theoretical Background

This chapter introduces the physical concepts that stand behind the operation of this thesis work. A description of the laser-induced phosphorescence along with the phosphor used is provided. The detectors employed in the experiment are described and their mechanism of operation is given.

2.1 Laser Induced Phosphorescence (LIP)

The demand on accurate temperature measurement is found in different fields such as industrial applications and scientific development. Thermographic phosphors provide a nonintrusive and remote method for accurate temperature measurement. All these advantages made thermographic phosphors the ideal substitute to other classical measurement methods such as thermocouples and other invasive temperature measurement techniques [1]. The applications and methods related to thermographic phosphors are extensively studied and presented in detail [2, 3].
Laser induced phosphorescence technique is divided into two sub categories, the first depends on the phosphor decay time for temperature evaluation, while the second method utilizes the fact that some phosphors have emission spectra that change as a function of temperature and the intensities ratios are used for temperature determination [4, 5]. In figure 2.1, different thermographic phosphors (both decay-time (blue scale) and intensity ratio (green scale) phosphors) are presented with different temperature sensitivity ranges.

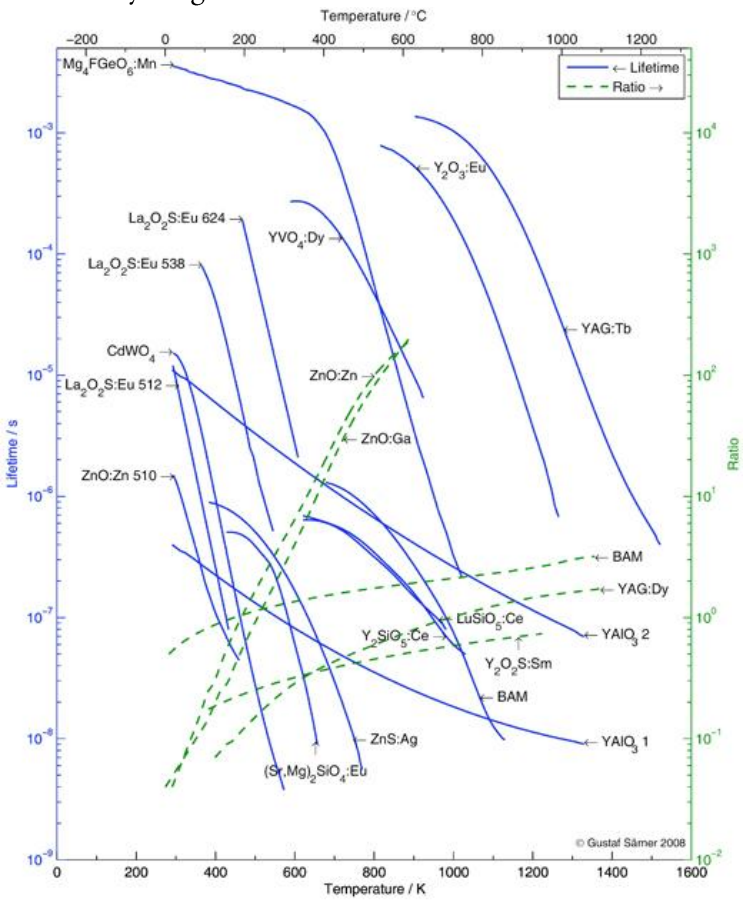

Figure 2.1: Temperature sensitivity ranges for different phosphors [6].

For the decay time method, the decay time decreases with increasing temperature. In order to find the correct phosphor temperature calibration is needed. Phosphor calibration is a technique used for each phosphor used to obtain a polynomial that describes the change of decay time as function of temperature. The accuracy of the calibration process is vital for high accuracy temperature determination in experiments due to the fact that any errors embedded in the calibration will propagate to the measurement and lead to faulty temperature evaluation.

2.1.1 Temperature measurement using LIP applied on $CdWO_4$

$CdWO_4$ or known as Cadmium tungstate is a very popular scintillator material due to its large absorption coefficient and quantum efficiency [7-11]. Cadmium tungstate has a wide absorption band and broad emission that is centered around 470 nm [9]. The excitation and emission spectrum of $CdWO_4$ is provided in figure 2.2.

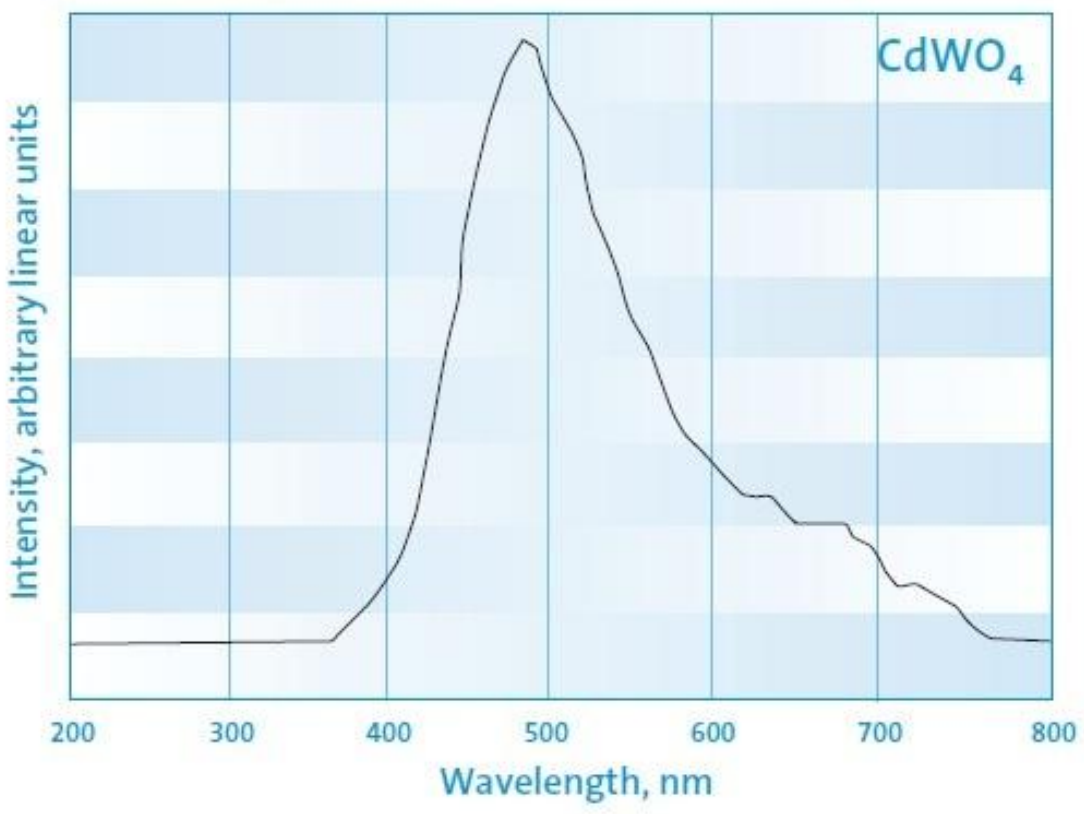

Figure 2.2: Cadmium Tungstate emission spectrum [12].

Temperature calibration is done for $CdWO_4$ phosphor and the resulting plot is shown in figure 2.3. The relation between the phosphor decay time and temperature is inverse, that means as the temperature increases the decay time decreases. Interpolation is used to fill out gaps in between measurement points to acquire a calibration polynomial. Also, phosphorescence intensity decreases with increasing temperature. A calibration polynomial is phosphor specific because each phosphor has a temperature sensitivity range as shown in figure 2.1. The dynamic range of the $CdWO_4$

phosphor stretches from room temperature up to 300 °C. This range is suitable for low temperature measurements; if high temperatures are needed to be measured, another phosphor should be chosen.

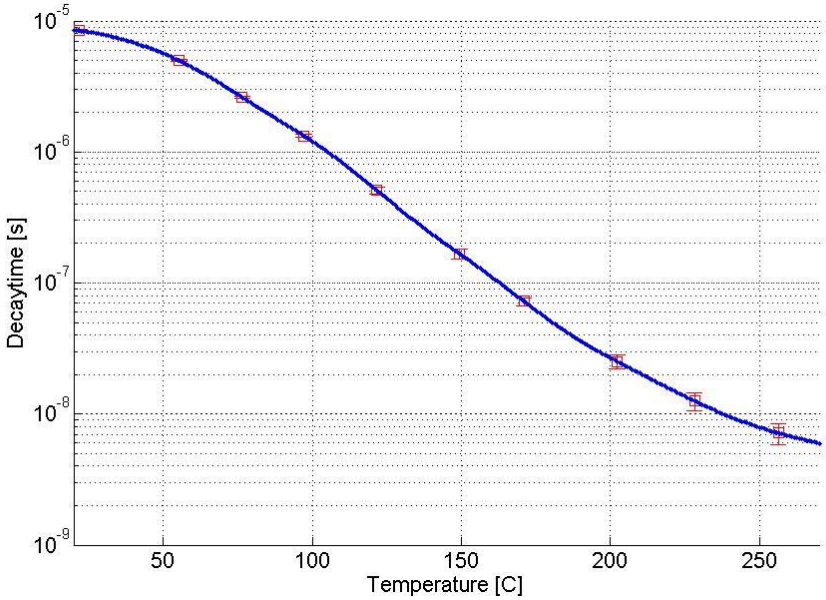

Figure 2.3: $CdWO_4$ phosphor temperature calibration curve.

2.1.2 Fixed window decay-time evaluation method

Phosphor decay time is of exponential nature and a fitting routine was written (by Christoph Knappe) to automatically evaluate the exponential decay constant τ. The evaluation code is written with the help of the article [13-15]. Exponential phosphorescence decay can usually be described with equation 2.1

$$I(t) = Ae^{-t/\tau} + B \qquad 2.1$$

where τ is the decay time, A and B are constants.
Actually, the phosphorescence decay is may be multi-exponential to some extent. For simplicity, it is assumed that the decay is single exponential and described by equation 2.1. The written code takes the first guesses of τ, A and B then it fits the decay curve with the least-squares method. First guess values are obtained using Ashworth's baseline rapid lifetime determination method (BRLD). The BRLD divides the exponential decay into three regions that have an equal width Δt and the areas covered by these regions are described by integrals which are denoted D_0, D_1, D_2.

$$D_0 = \int_0^{\Delta t} \left(Ae^{-\frac{t}{\tau}} + B\right) dt$$
$$D_1 = \int_{\Delta t}^{2\Delta t} \left(Ae^{-\frac{t}{\tau}} + B\right) dt \qquad 2.2\text{ (a, b, c)}$$
$$D_2 = \int_{2\Delta t}^{3\Delta t} (Ae^{-t/\tau} + B) dt$$

τ, A, B are given by:

$$Y = \frac{D_1 - D_2}{D_0 - D_1} \tag{2.3}$$

$$\tau = \frac{-\Delta t}{\ln Y} \tag{2.4}$$

$$A = \frac{(D_0 - D_1)\ln Y}{-\Delta t(1 - Y)^2} \tag{2.5}$$

$$B = \left[D_0 - \frac{D_0 - D_1}{1 - exp(-\frac{\Delta t}{\tau})} \right] \times \frac{1}{\Delta t} \tag{2.6 (a, b)}$$

$$B = \left[D_0 - \frac{D_1 - D_2}{1 - exp(-\frac{\Delta t}{\tau})} \right] \times \frac{1}{\Delta t}$$

The least squares fitting code uses fixed window method for decay time calculation. This means that the beginning and the end of the fitted section of the decay have to be set manually. Setting the start of the window and the end of the window assures similar fitting conditions for curves measured at the same temperature. This is important to rule out the effect of the fitting routine in temperature deviation.

2.2 Optical detectors

Phosphor decays are registered using optical detectors that convert the photons into electrons that can be read and saved using an oscilloscope. In this thesis, four different detectors are used to provide variation of amplification and sensitivity ranges. Also two of the detectors are time gated, thus providing an insight into comparison between gated and normal mode detectors.

2.2.1 Photomultiplier Tube

Due to its fast response and high sensitivity, the photomultiplier tube is a versatile photo-detector. PMTs are mainly composed of a photocathode, electron-focusing electrodes, dynode chain, and anode as shown in figure 2.4. The photocathode is a photosensitive layer that has a very low work function in order to emit electrons after the absorption of photons. The released electrons are then accelerated under an applied potential towards the first dynode. Upon impact, the electrons release secondary electrons and then these electrons impinge onto the next dynode under the effect of applied voltage (around 100V) and release more electrons. This process is repeated across the chain of dynodes that can contain up to 13 dynodes [16], resulting in the amplification of the original electrons by a large factor typically ranging from 10^3 to 10^8 [16, 17]. The electrons are then collected by the anode grid providing an output current. [16-18]

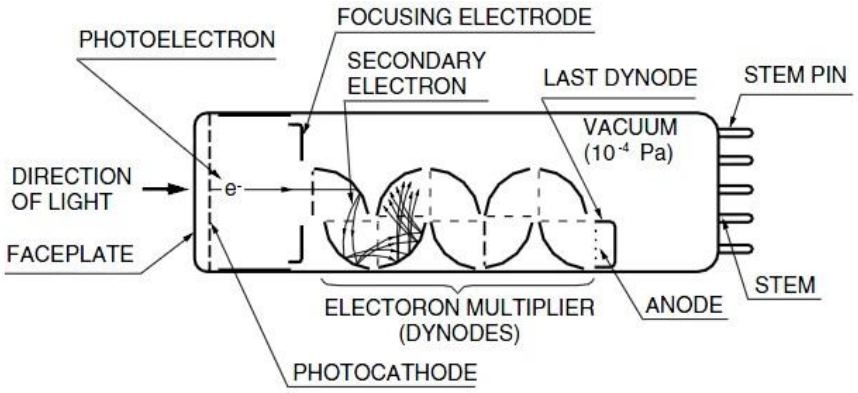

Figure 2.4: Main components of a photomultiplier tube [16].

2.2.2 Avalanche Photodiode

Avalanche photodiodes (APDs) are characterized by their high sensitivity, high speed and internal gain mechanism. APDs are able to detect a low light level with detection ranges extending from the infra-red down to visible region of the radiation spectrum [19, 20].
The impact of photons on a photodiode (hitting the P-side of the P-N junction) yields electron hole pairs in the case when the energy of the photons is greater than the band gap energy of the semiconductor material used in the photodiode. The silicon (Si) photodiodes are sensitive to light with wavelength shorter than 1100 nm due to the fact that the band gap energy of Si is 1.12 eV. In the depletion area when a potential is applied the electrons accelerate towards the N-side while the holes accelerate towards the P-side of the PN- junction. Under the effect of a sufficient applied potential the carriers accelerate and gain enough energy that when they collide with the crystal lattice they create a new electron-hole pair. The newly created pairs will collide also in the crystal lattice and release even more electron-hole pairs. This phenomenon is known as avalanche effect and acts as the amplifying mechanism on the Si APDs (figure 2.5).

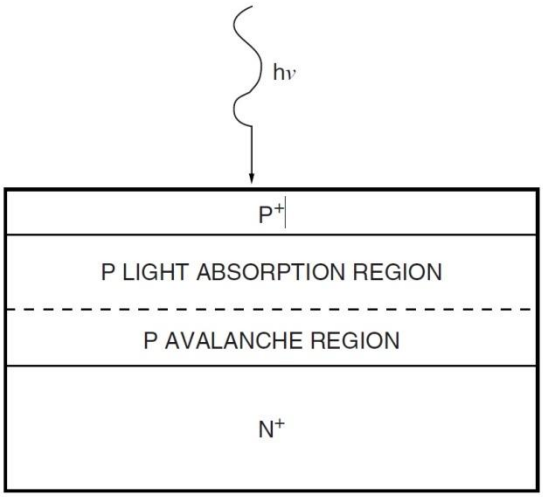

Figure 2.5: Avalanche process in a photodiode [19].

Increasing the reversed voltage leads to increase in the gain of the APD. In addition, the gain is inversely dependent on the temperature because as the temperature increases the vibration of the lattice increases leading to the collision of the carriers before they have reached high energies to generate new electron hole pair.

2.2.3 Micro-channel Plate Photomultiplier Tube

A micro-channel plate Photomultiplier tube (MCP-PMT) is another type of photo-detector that works in a similar way as a normal PMT except for the fact that the dynode chain present in the PMT is replaced by a micro-channel plate. The MCP is a thin disc of bundled, parallel aligned glass channels that have a typical diameter ranging from 6 to 20 micrometers [18]. Each individual channel acts as electron multiplier. The principle behind the multiplication process is illustrated in figure 2.6

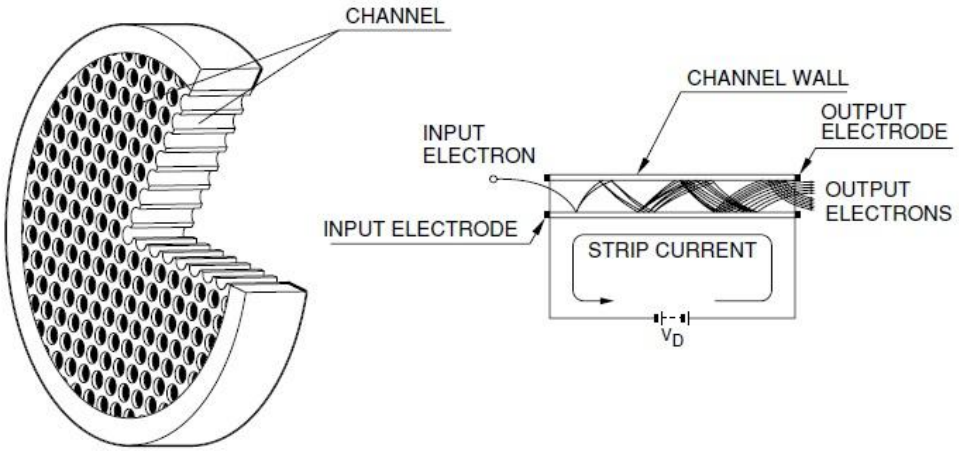

Figure 2.6: Micro-channel plate and electron multiplication process [18].

Electric field is applied across the MCP and electrons are accelerated under the field, which lead the electrons to collide with the inner walls of each channel, generating secondary electrons. This process is repeated along the MCP where more secondary are emitted by electrons impinging on the MCP wall. The result of this process is a large number of electrons reaching the output end of the MCP. MCP PMTs have a number of characteristics that make them unique such as fast time response (fraction of ns), high gain (up to 10^8), wide bandwidth measurement (down to picoseconds level) [18], and high optical sensitivity.

2.3 Nonlinearity in Detectors

Linearity in a photodetector is defined as the linear relation between the input and the output of the detector. The input of a photodetector is the number of photons impinging the detector window and the photocathode to create electrons, while the output of such a detector is the output current generated after the multiplication of the electrons [21-26]. Such a detector can be

operating in three modes, the first is proportional linear mode, the second is linear mode and the third is nonlinear mode as illustrated in figure 2.7.

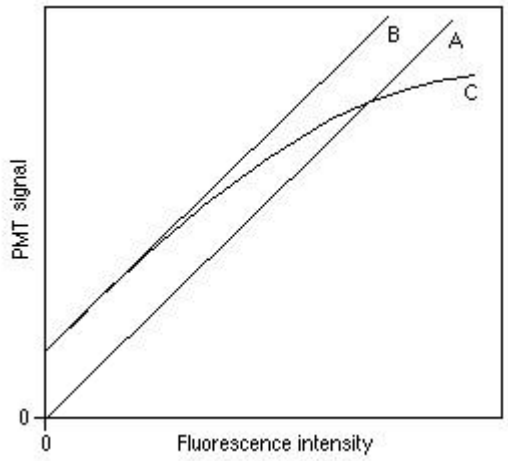

Figure 2.7: Photodetector response modes (A: linear proportional, B: linear, C: nonlinear) [21].

A proportional linear relation (A) between the input and the output of the photodetector means that the output is only a constant factor multiplied by the input. That means the output is resulting from a multiplication constant multiplied with the input with a constant offset. The nonlinear case (C) has a linear relation at low input intensity, but as the input increases to high levels the relation deviates from linearity and provides less or more output than it should in the ideal case. Nonlinearity in photodetectors results from saturation either in the photocathode (optical saturation) or from saturation in the multiplication and collection of electrons.

2.3.1 Optical saturation

Photodetectors are detectors that capture photons and convert them in to electrons that are then multiplied and collected to form an electrical signal as an output. The first step is the photon- to electron conversion that takes place in the photocathode. The created photoelectrons accelerate towards the multiplication region. If high intensity light hits the cathode, a large number of photons collide with the photocathode in a short time leading to depletion in the photocathode. The photocathode depletion means that the number of generated photoelectrons is no longer proportional to the number of colliding photons. In this case, the photocathode is said to be saturated and thus the detector response has deviated from ideal linear case. In order to avoid optical saturation of photocathode, the intensity levels of incoming light should be lower than the depletion limit.

2.3.2 Electrical saturation

Similar to the case of the optical saturation, electrical saturation also occurs in the multiplication process in the photodetector. The multiplication process in photodetectors differs in mechanism from one detector type to another. PMTs utilize a dynode chain in which the electrons collide with the dynode surface releasing secondary electrons. These dynodes have an electrical voltage

applied across them provide enough acceleration for the electrons to create secondary electrons. In MCP-PMTs, the electrons multiply by hitting the inner wall of the micro-channels, which have an electric potential applied across its terminal. APDs have an internal multiplication mechanism known as the avalanche process in which carriers accelerate under the effect of the reverse voltage and hit the crystal lattice generating secondary electron-hole pair.
If a large number of photoelectrons is generated at the photocathode, saturation of the electron multiplication mechanism elements (dynodes, MCP, crystal lattice) and anodes occurs. The saturation results from the incapability of the electron amplification unit to produce a proportional amount of additional electrons as new electrons continue to enter. For this case, the relation between the primary photons and emitted secondary photons is no longer linear and the device enters a state of saturation. Detector manufactures assign a maximum output current for which the detector is supposed to operate linearly.

2.3.3 Photomultiplier tube linearity

PMTs are deployed in various fields of study and research extending from astrophysics to recent medical devices. Several factors such as divider current and space charge can affect the linearity of a PMT. This sub-section discusses in detail the linearity of the PMT photodetector and the various factors that affect its linearity.[16-18, 25]

Divider Current
Electron multiplication in the PMT is done by a dynode chain that contain from 6 to 13 dynodes. In order to obtain secondary electron emission form the dynodes, an electric potential is applied to the dynode. The voltage is divided on the dynode chain using a voltage divider circuit that is composed of series of resistors (figure 2.8).

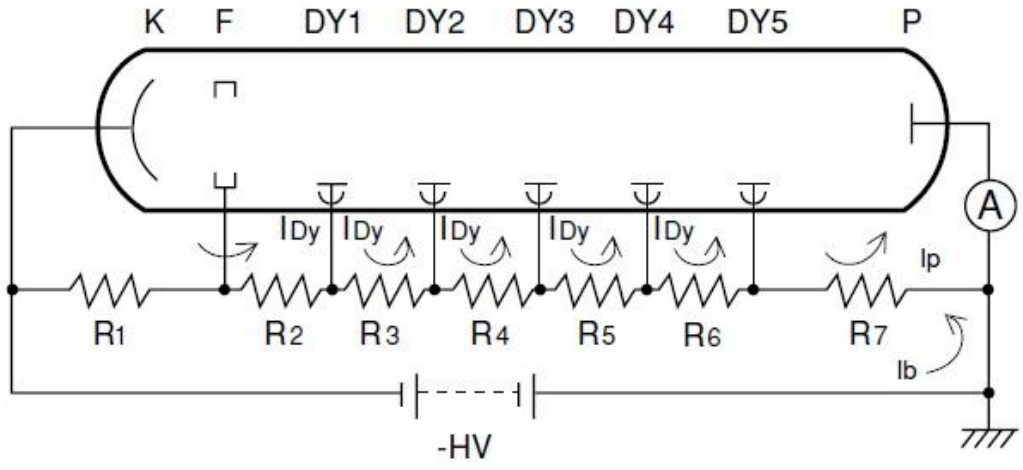

Figure 2.8: PMT voltage-divider circuit K (Cathode), F (electron focusing), DY (dynode), P (Anode), R (resistor), HV (high voltage), I_{DY} (dynode current), I_P (anode current), I_b (divider current). [18]

The applied high voltage across the photomultiplier ranges from 500 to 3000 V. The dynode inter-stage voltage is specified for each dynode using different resistance (100 kΩ - 1MΩ). The voltage divider current has an effect on PMT linearity as indicated in figure 2.9. At low level of incident light the PMT has a linear response (region A), but when a specific incident light level is reached the PMT response deviates from linearity (region B). As the level of incident light increases, the PMT then inters a state of saturation (region C) [18].

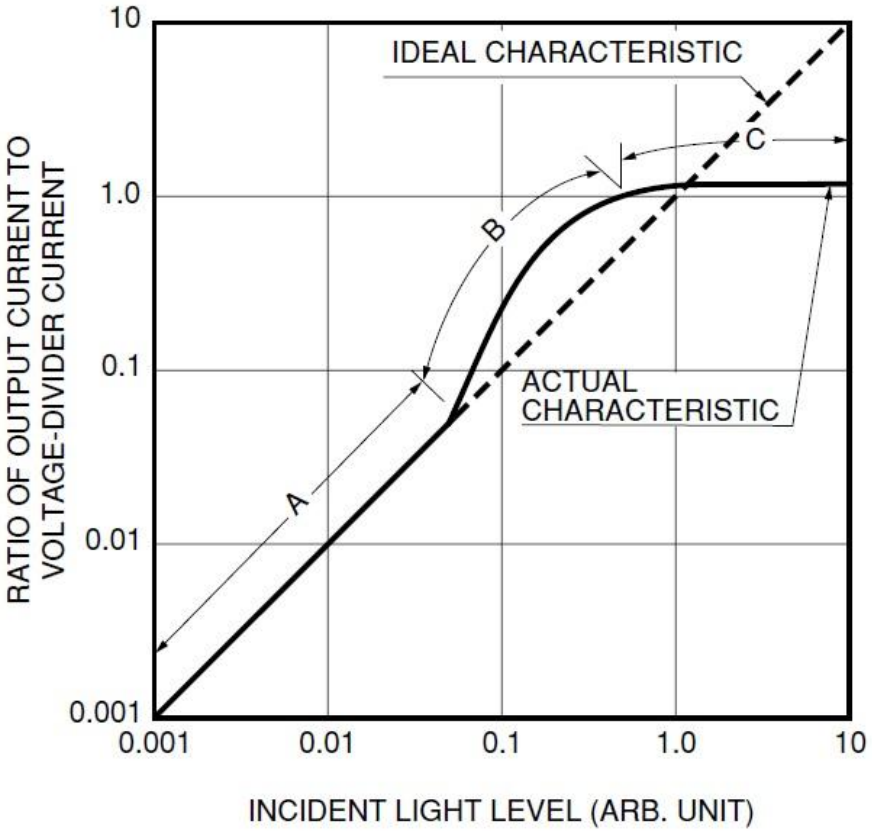

Figure 2.9: PMT output linearity, region A: Linear, region B: nonlinear, region C: saturation.[18]

To understand the principles behind the nonlinear behavior of the PMT, the relation between the dynodes' current and the anode current should be revealed. The current through the last dynode resistor is the difference between the voltage divider current and the anode current. However, the current through the other resistances are the difference between the voltage divider current and the dynode current. The dynode and anode currents flowing reduce the divider current. The dynode current of the first dynode is lower than the dynode current of the successive dynodes. The increase of the dynode current results in significant loss in the inter-stage voltage applied across the dynode. For small anode output currents, the inter-stage voltage loss can be ignored and its effects are insignificant. As the level of incident light increases, the anode and dynode current increases and the inter-stage voltage losses become more significant as illustrated in figure 2.10.

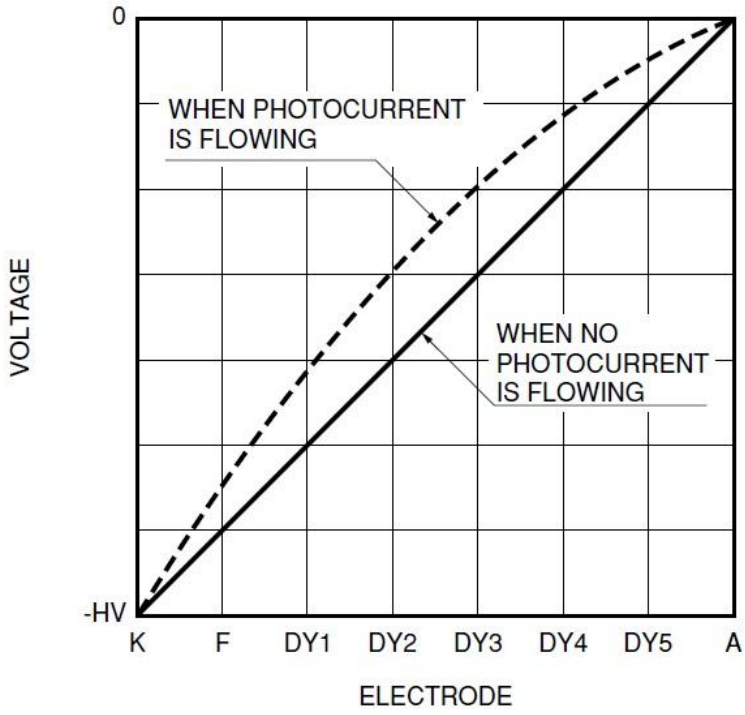

Figure 2.10 : Effect of photocurrent flow on Interstage voltage.[18]

The high voltage power supply maintains the anode and the cathode to a constant voltage. Due to this fact, the loss of the inter-stage voltage in one dynode leads to redistribution or compensation in the previous dynode and similar action takes place in the other dynodes. This compensation results in the increase of the inter-stage voltage. The cumulative increase of inter-stage voltages, leads to increase in the current amplification as visible in figure 2.9. The most significant loss of inter-stage voltage occurs between the last dynode and the anode. With further increase in the level of the incident light, the anode generates large anode output current. The large anode output current causes a severe drop in the inter-stage voltage between the anode and the last dynode. Then the collection efficiency of the anode drops, that lead the PMT to enter a state of saturation. For DC operation the linearity can be improved either by introducing a Zener diodes between the last dynode and the anode, or to lower the resistance of the resistors of the voltage divider circuit to provide more voltage divider current. For Pulse operation linearity increase, the last couple of dynodes are connected to decoupling capacitors that provide the dynode with electric charge to prevent the voltage drop through the inter-stage voltage divider. In addition, the installation of individual voltage supply for each component can replace the voltage divider circuit and extend the linearity of the PMT.

Space charge

Space charge plays a role in the linearity of the PMT at high currents. The space charge effect on linearity is highest in the areas of high current densities, that is the last few dynodes and the anode area. The change in electron trajectories decrease the multiplication process yield and anode collection efficiency. To minimize space charge effect on anode collection efficiency, the anode is placed close to the last dynode. Placing the anode close to the last dynode causes the last dynode to act as a fractional electrostatic shield to the anode collection surface.

3. Experimental Methods

This chapter provides details on the experimental setup used in the measurements done in this thesis work. The setup component details are presented along with operation conditions under which the experiment was completed. In addition, the reference system design for the measurement of the number of incident photons is illustrated.

3.1 Experimental Setup

The setup used for the work presented here is composed of the excitation radiation source (Nd:YAG laser @ 266 nm), Detectors (Hamamatsu H6780-04 photomultiplier tube, Hamamatsu H11526-20-NF time-gated PMT, Hamamatsu S5343 Si-APD, Hamamatsu R5916U-50), radiating material (thermographic Phosphor: $CdWO_4$), Optical components (Interference filters, dichroic mirrors, lenses, quartz plate). The setup is represented in figure 3.1

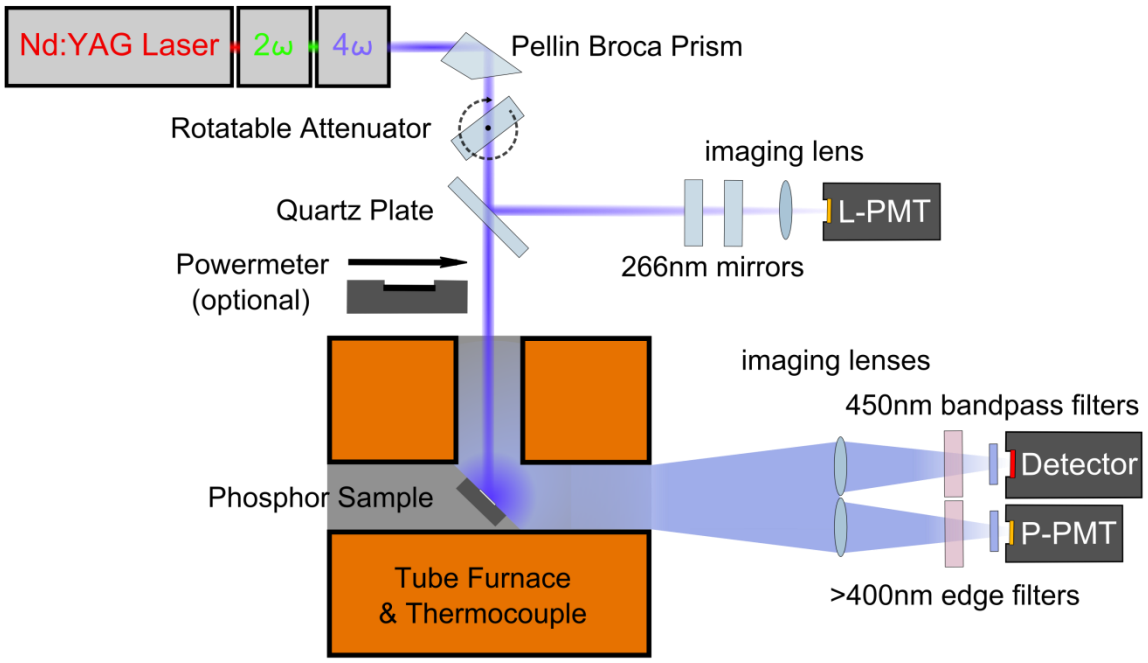

Figure 3.1: Experimental setup [27].

The laser beam emitted by the laser contains the three wavelengths (266, 532, and 1064 nm). Using a prism the three wavelengths are separated and the 266nm laser beam is remaining after dumping the other laser beams on an optical dump. Then the laser beam continues towards a quartz plate where a fraction of the beam is reflected towards the laser reference PMT. The laser beam is then directed to hit the phosphor plate placed inside the furnace. When a laser pulse excites the $CdWO_4$, phosphorescence is emitted from the plate. The phosphor plate was placed at almost 45 degrees so it could be excited from the furnace side. The phosphor plate is placed in the oven and heated up to different temperatures and then matrix measurements are taken by holding the gain constant and scanning the laser pulse energy starting from maximum laser pulse energy to minimum energy. Two plano-convex lenses are used to focus the phosphorescence

radiation onto the detectors. The first lens focuses the phosphorescence on the phosphorescence intensity reference PMT. The reference PMT measures the phosphorescence intensity as the laser pulse energy is scanned during phosphor excitation. While the second lens focuses the phosphorescence onto the detector that measures the phosphorescence decay time. A reference system was built in the setup to measure the relative laser energy and the number of photons reaching the detector. This system and its working principles will be presented later in section 3.4.1. The reference system uses two PMTs of the same module as detection elements and for signal intensity measurements in relevance to the phosphorescence and laser energies. In order to prevent unwanted laser radiation or scattered light from entering the detector two sets of filters are placed in front of the detector. The first filter is an interference filter with central acceptance wavelength band of 450 nm ± 20 nm, while the second filter is a high wavelength edge filter with acceptance wavelengths greater than 400nm.
Then the oscilloscope using the 50-Ω termination registers the signal produced by the two reference PMTs and the detector. The two reference PMTs are kept at the same gain value (gain= 6300) for whole duration of the experiment regardless of the detector used.

3.2 Laboratory Equipment

3.2.1 Nd:YAG Laser

The $CdWO_4$ is excited using laser radiation (@ 266 nm) produced by q-switched Quantel Brilliant B pulsed Nd:YAG laser operating at 10 Hz. The laser produced four different laser wavelengths (1064, 532, and 266 nm) using the suitable harmonic generator unit. In this investigation the laser wavelength of 266 nm is produced using the frequency-doubling unit (2ω) followed by frequency quadrupling unit (4ω) as illustrated in figure 3.2. The emitted laser pulses have pulse duration of approximately 5 ns. The maximum energy per pulse for each of the wavelengths is: 850 mJ @ 1064 nm, 400 mJ @ 532 nm, and 90 mJ @ 266 nm [28]. During the measurements, the maximum laser energy per pulse was limited to a maximum of 5.0 mJ.

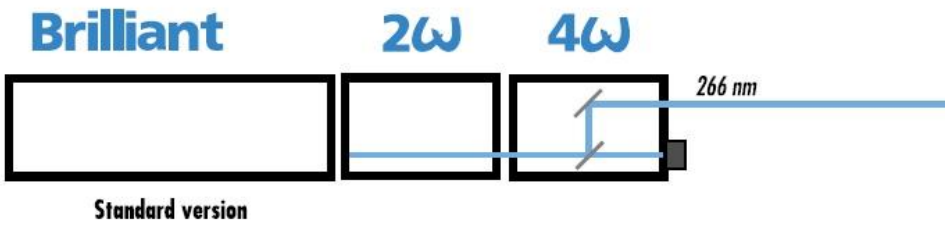

Figure 3.2: Q-switched Nd:YAG laser producing 266 nm radiation [28].

3.2.2 Oscilloscope

To measure the phosphorescence signal acquired by the detectors, LeCroy WaveRunner 6030A Oscilloscope was used. The oscilloscope has a maximum sampling rate of 2.5 GS/s that

corresponds to 400 ns separation between two consecutive measuring points. The sampling rate during the measurement was modified to have the highest possible resolution taking into consideration the saved file size. All of the four oscilloscope channels were used to acquire the signals coming from the measurement and reference detectors. The first channel measured the signal generated by the laser reference PMT. The second channel measured the signal produced by the phosphorescence reference PMT. The third channel registered the signal coming from the detector that measured the phosphor exponential decay. Finally, the fourth channel was deployed to acquire the trigger signal produced from the laser q-switch. The signals registered in the first three channels of the oscilloscope were saved as binary file (.trc file extension). All of the signals were measured over a channel termination of 50-Ω.

3.2.3 Thermocouple

Thermocouples are temperature-sensing devices that are composed of two different conductor material that are joined at the sensing end of the thermocouple. As the thermocouple gets heated or cooled, a voltage is produced that is related to the measured temperature. There are different thermocouple types available depending on the material used in the thermo couple manufacturing. The most commonly used types are J, K, E, and T. The thermocouple used in the temperature calibration of the $CdWO_4$ is of type-K. Type-K thermocouples are composed of the two alloys chromel (90% nickel, 10% chromium) and alumel (95% nickel, 2% manganese, 2% aluminum, 1% silicon) and have a temperature sensitivity range from -200 to 1300 °C.

3.2.4 Power-meter

Laser power measurement is necessary to avoid subjecting the $CdWO_4$ phosphor to an excess of laser power that might damage the coated phosphor. In addition, the power meter is used as a key element in the calibration of the reference system for the measurement of the number of photons (section 3.4.1). The absorbing layer of the power meter converts the laser power into heat that is measured and laser beam power is given. The power meter used is an Ophir Nova II measuring unit that has accompanying software installed on the oscilloscope.

3.2.5 Current to voltage Amplifier

To avoid PMT saturation during phosphorescence detection, PMT gain is lowered and an amplifier circuit is needed to compensate for the gain drop. The current to voltage amplifier implemented is in-house built. Converting the signal from current into voltage means that that signal can run through long cables without being heavily affected by the cable's capacitance. The used amplifier converts the current output signal of the PMT into amplified voltage. To calculate the amplification factor of the amplifier used a PMT signal (run under normal mode of operation) of 5 mV amplitude. By taking into consideration that the oscilloscope has a termination of 50 Ohm, the signal current output is 100 μA. Then the PMT is run under the same gain and same input intensity level but the PMT was run under Amplified mode of operation. The resulting voltage output measured by the oscilloscope is 120 mV. Using the formula of the current to voltage amplifier (Equation 3.1) the resistance can be calculated and the amplifier gain is found.

$$V_{Out} = I_{in} \times R$$
$$R = \frac{V_{Out}}{I_{in}} = \frac{0.12V}{1 \times 10^{-4}A} = 1200\ \Omega \quad (3.1)$$

This means that the current signal is multiplied by 1200 and converted to voltage. A 2V signal measured by the oscilloscope is originally a 40 mA PMT current output signal read over a 50-Ω oscilloscope termination. To produce the same output voltage signals using an amplified PMT only a current output signal of 1.67 mA is needed because of the amplification factor of 1200 provided by the amplifier. This comparison between the normal an amplified modes of operation indicates that the PMT can be run under low gain when operated under amplified mode of operation and as a result avoiding saturation. The used amplifier is in-house built and it suffers from narrow bandwidth limited to 5 MHz, which creates a broadening in the amplified signal (200 ns time-scale broadening). This means that the generated signals at high temperatures (decay-time < 200ns) are largely affected by the broadening.

3.2.6 Photomultiplier Tube

The PMT used is Hamamatsu H6780-04 with a spectral response range 185-850 nm. The detector characteristics are listed in table 3.1.

Table 3.1: Hamamatsu H6780-04 Photomultiplier tube specifications

Specification	Value	Unit
Spectral response	185-850	nm
Peak sensitivity wavelength	400	nm
Maximum output signal current	100	μA
Cathode radiant sensitivity	60	mA/W
Anode radiant sensitivity	3×10^4	A/W
Anode luminous sensitivity	75	A/lm
Rise time	0.78	ns

3.2.7 Time-gated Photomultiplier Tube

The time-gated PMT used in the measurement is Hamamatsu H11526-20-NF and its specifications are listed in table 3.2. The NF characters in the module name stands for gate mode is Normally Off (NF). The NF gate mode means that the PMT stays turned off until it is triggered to operate by an input gate signal.

Table 3.2: Hamamatsu H11526-20-NF time.-gated Photomultiplier tube specifications

Specification	Value	Unit
Spectral response	230-920	nm
Peak sensitivity wavelength	500-700	nm
Maximum output signal current	100	μA
Cathode radiant sensitivity	78	mA/W
Anode radiant sensitivity	1.5×10^5	A/W
Anode luminous sensitivity	1000	A/lm
Rise time	0.57	ns
Rise time (Gate Mode)	70	ns
Gate signal pulse width	100ns to DC	--
Gate mode delay time	180	ns

3.2.8 Micro-channel Plate Photomultiplier Tube

A Hamamatsu R5916U-50 MCP-PMT is deployed in the experiment and specifications are in table 3.3

Table 3.3: Hamamatsu R5916U-50 micro-channel plate Photomultiplier tube specifications

Specification	Value	Unit
Spectral response	160-850	nm
Peak sensitivity wavelength	430	nm
Maximum output signal current	350	mA
Cathode radiant sensitivity	50	mA/W
Rise time	180	ps
Rise time (Gate Mode)	1	ns
Gate signal pulse width	5 to 10000	ns

Since the maximum input gate width is limited to 10 μs, decay-times longer than 2 μs are not detectable. The time gate maximum width limit restricts the MCP-PMT measurement for the $CdWO_4$ phosphor for temperatures higher than 100 °C.

3.2.9 Avalanche Photodiode

The avalanche photodiode module implemented in the experiment is Hamamatsu S5343 Si-APD. The APD gain was changed by changing the reverse voltage applied to it. However, the APD suffers from low gain range compared to the other used detectors that have large gain ranges.

Table 3.4: Hamamatsu S5343 Si-APD specifications

Specification	Value	Unit
Spectral response	200-1000	nm
Peak sensitivity wavelength	620	nm
Quantum efficiency	80 (@ 620 nm)	%
Break-down voltage	150	V

3.3 Detector gain ranges and measurement temperatures

The decay-time range of the $CdWO_4$ phosphor that extends over [5ns-15μs], that has determined the measurement temperatures [21-290 °C] for this thesis work. The temperatures chosen for the measurement are at temperatures [21, 100, 181, 246, 288] °C measured by a thermocouple inside the oven (not attached to the phosphor sample). All detectors have measurements taken at each of the listed temperature points except for the MCP-PMT where the room temperature measurement is missing due to the limitations on the gate input signal width. In order to build a detector response matrix gain has also to be changed and a suitable gain range was chosen for each detector (Table 3.5).

Table 3.5: Detector gain ranges

Detector	Gain Range
PMT Normal mode	480 - 43000
PMT Amplified mode	42 - 80
Time-gated PMT	950 - 7700
MCP-PMT	36 - 3000
Si-APD	62 - 470

The gain range was chosen by having the laser at maximum energy per pulse of 5.0 mJ. To determine maximum gain, the gain is increases until a phosphorescence signal peak voltage of 2 V, is obtained for the two PMT devices. For the minimum gain is set at a phosphorescence signal peak voltage of 0.3 V. From experimental trails, starting a matrix with a maximum signal lower 0.3 V will lead to a large number of empty cells at lower laser intensities. Due to the limited gain range for the Si-APD, the gain range maximum was chosen just below the breakdown voltage (156 V @ room temperature). The gain range displayed in table 3.5 was fixed for each detector and did not vary as temperatures were changed.

3.4 Measurement methods

3.4.1 Reference system for number of photons computation

Detector response matrices were created for different temperature that illustrate the evaluated phosphorescence decay time as a function of detector gain and amount of photons, hitting the detector per time interval. This matrix illustrates the way the detector behaves under the specified photons number and gain ranges. During a single temperature measurement, the gain is changed in steps and a matrix row is measured by scanning the laser energy that excites the phosphor. Laser energy is altered using a dichroic mirror that varies its transmission as function of the incident angle of the laser beam. The dichroic mirror is mounted on a precise rotating stage that scans over a range of angles leading to laser energy scan and thus phosphorescence intensity scan. The laser intensity was dropped from a maximum of 5.0 mJ down to 70 μJ by dichroic mirror rotation.
In order to achieve a common reference that can be used for all of the detectors regardless of their operation modes, the amount of photons reaching the detector is calculated (figure 3.1). Using a quartz plate, a reflection of the laser radiation (@ 266 nm) is directed towards a Hamamatsu H6780-04 photomultiplier tube. The laser beam was heavily attenuated using two highly reflective dichroic mirrors @ 266 nm to prevent PMT damage, then the beam is focused onto the PMT using a plano-convex lens for full collection. By varying the laser energy and registering the value of the signal generated by the PMT, a relation was drawn between the measured laser energy per pulse (J) and the generated PMT signal (V). In matrix measurements the laser energy per pulse was scanned from a maximum of 5mJ down to 15μJ. Fitting of the resulting relation is provided in figure 3.3. The figure 3.3 shows that the PMT response is nonlinear as function to the laser intensity, but this behavior will not change because that PMT is ran under constant gain.

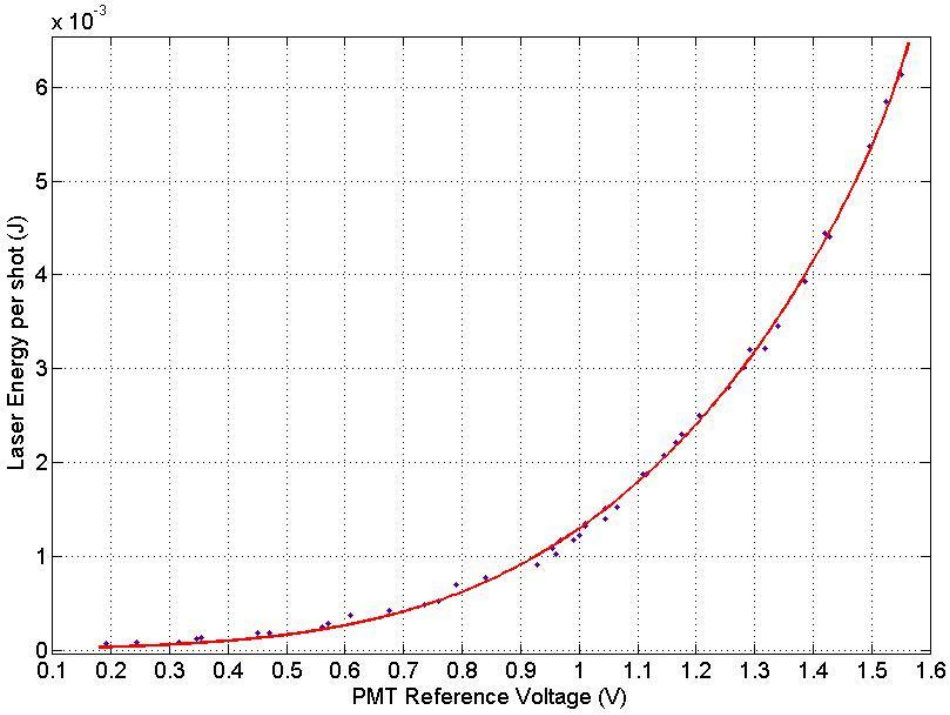

Figure 3.3: Laser energy per shot as function of PMT reference voltage at PMT gain 6300.

The laser pulse energy is the energy exciting the phosphor and as shown in figure 3.3, the PMT response is saturated. The relation is best fitted by a Gaussian function described in the equation below:

$$F(x) = A_1 e^{-(x-B_1/C_1)^2} + A_2 e^{-(x-B_2/C_2)^2} + A_3 e^{-(x-B_3/C_3)^2} \quad 3.2$$

F(x) = Laser energy per shot
x = PMT reference voltage

The Gaussian fit coefficients are provided in table 3.6:

Table 3.6: Gaussian fit coefficients

A_1	0.009399	B_1	1.815	C_1	0.134
A_2	0.01543	B_2	2.367	C_2	0.8764
A_3	-0.000468	B_3	1.515	C_3	0.3598

Then using the following relation the number of photons per pulse is found (Equation 3.3):

$$Photons\ per\ pulse = \frac{E_{Pulse} \times \lambda}{h \times c} \quad 3.3$$

h = Planck's Constant
c = Speed of light in vacuum

The two reference PMT (measuring laser intensity and phosphorescence intensity) are held at the same gain. To be able to apply the formula for the Phosphorescence number of photons the same relation is used taking into consideration the PMT sensitivity difference at the Laser wavelength (266 nm) and at the phosphorescence wavelength (450 nm). The ratio of the PMT sensitivity (Ratio = 0.8) at the two wavelengths is used in the new relation. Thus, the final calculation is:

$$F(0.8x) = A_1 e^{-(0.8x-B_1/C_1)^2} + A_2 e^{-(0.8x-B_2/C_2)^2} + A_3 e^{-(0.8x-B_3/C_3)^2} \quad 3.4$$

To convert from the laser energy to number of photons hitting the detector several factors should be taken into consideration such as Quartz plate reflex (2.69%), HR dichroic mirrors (*T*=1.0% each), and lens multi reflections (*T*= 93.2%).
Error propagation through the calculations is necessary to find the margin of error and the extreme limits of the values found. Starting with the Gaussian fitting an error of around 5% is found and the other error sources and values are listed in the table below.

Table 3.7: Error soursces and percentage error.

Error source	Transmission	Percentage Error
Multi-reflex upon Q-plate	R=0.0268	0.56%
HR dichroic mirrors (x2) ($T_{Dichroic}$)	0.01	1.0%
Gaussian Fit	-	5.0%
Signal Multi-reflex on lens (T_{Lens})	0.932	1.0%
Total Error	-	8.6%

The total error is computed by the addition of all of the individual percentage error listed in table 3.7 taking into consideration that two dichroic mirrors are used. The error values for the dichroic mirrors listed in the table are found based on the data sheet provided by the manufacturer, while the lens multi reflex can be calculated using the derivation from Fresnel formulas of reflectivity (Equation 3.5) where n_0 and n_s are the refractive indices of air and quartz respectively:

$$R_{Multi} = \left(\frac{2R}{1+R}\right)$$

$$R = \left(\frac{n_s - n_0}{n_s + n_0}\right)^2 \qquad 3.5$$

$$n_0 = 1.0;\ n_s = 1.46$$

To be able to have transformation from the laser reference PMT voltage to energy relation, a small duration of time Δt should be introduced into the equation 3.6. Δt is a time interval sliced out from the middle of a Gaussian laser pulse in time. This will be the proportional part of the laser pulse that is seen as the maximum signal voltage of the laser reference PMT. In addition, a ratio between the reflection coefficient (R_Q) and transmission coefficient (T_Q) of the quartz plate is added to the calculation. The transmission coefficients of the two dichroic mirrors ($T_{Dichroic}$) and the plano-convex lens (T_{Lens}) are taken into consideration. The introduction of the FWHM of the laser beam in to the equation is to consider the Gaussian nature of the profile of the laser pulse.

$$E_{Phosp.PMT} = \frac{F(0.8x)}{\sigma\sqrt{2\pi}} \Delta t \frac{R_Q}{T_Q} T_{Dichroic}^2 T_{Lens} \qquad 3.6$$

$$\sigma = FWHM\ of\ the\ laser\ pulse = 5ns$$
$$\Delta t = time\ duration\ of\ photon\ population = 1\ ns$$
$$T = Transmission$$

$$Number\ of\ Photons_{Phosp} = \frac{\lambda_{450\ nm}}{h \times c} \times E_{Phosp.PMT} \qquad 3.7$$

Finally, the relation between the Phosphorescence PMT intensity and the Number of Photons is plotted and presented in figure 3.4. Using the plot in figure 3.4 the number of photons axis for the detector response matrix is created.

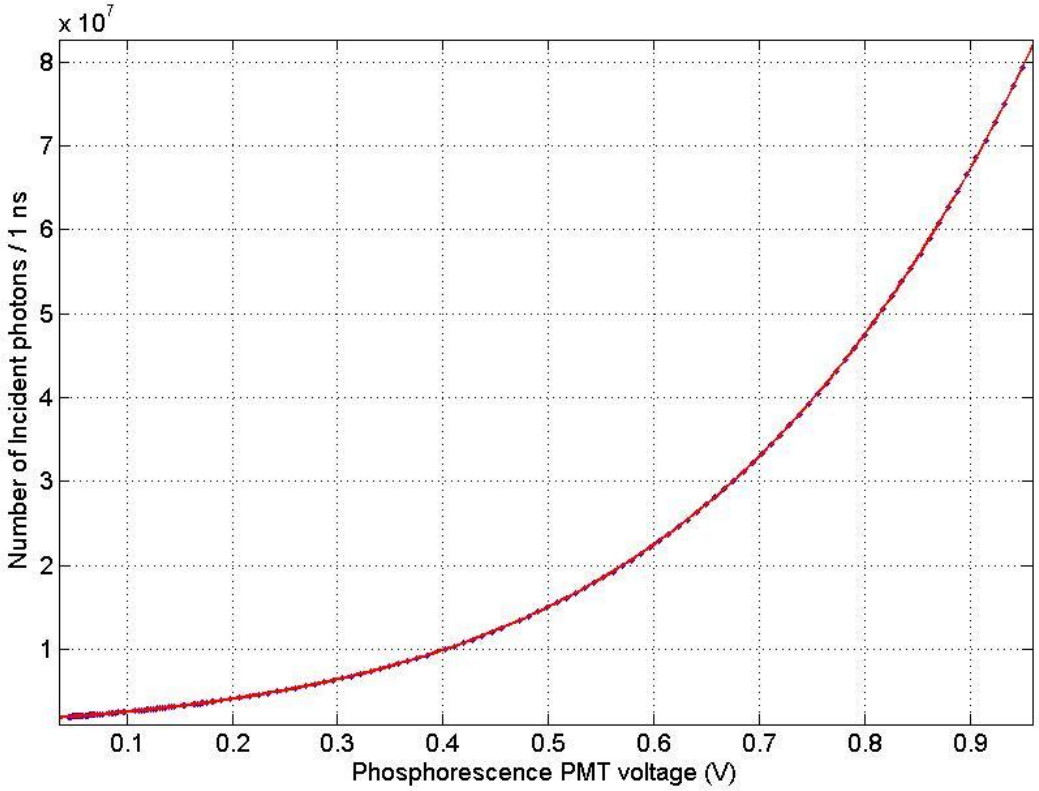

Figure 3.4: Relation of number of photons / 1 ns as function of Phosphorescence PMT signal Intensity at PMT gain 6300.

The number of incident photons per one ns as function of reference phosphorescence intensity is ranging between (0.1 - 8) × 10^7. The total percentage error will give the number of incident photon distribution minimum and maximum values at a constant light intensity.

4. Results

In this chapter, the results obtained for each detector are presented and sorted mainly by the detector type then subdivided by the mode of operation. The detector specific response matrices are represented as two-dimensional matrices (detector-gain and number of photons per 1ns) with the third dimension presented as color gradient of the information added. The third dimension information could be mean decay time, standard deviation, percentage error, number of averaged files in each single matrix element, and signal to noise ratio. The temperatures referenced are the oven temperature measured by the oven thermocouple. The K-type thermocouple temperature is higher than the phosphor temperature.

4.1 Linearity response of a PMT: Hamamatsu H6780-04

4.1.1 Normal PMT mode

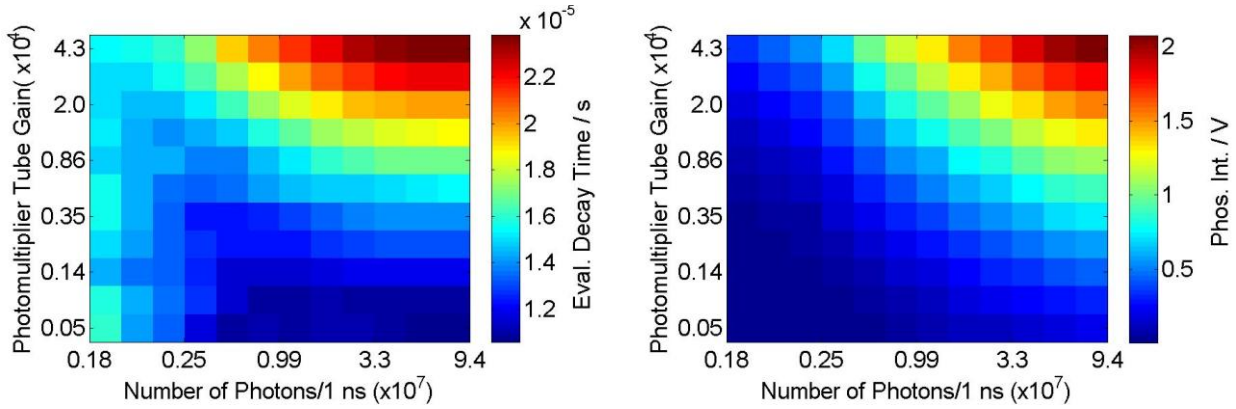

Figure 4.1: PMT in normal mode at T=21 °C, decay time (left) and phosphorescence intensity (right).

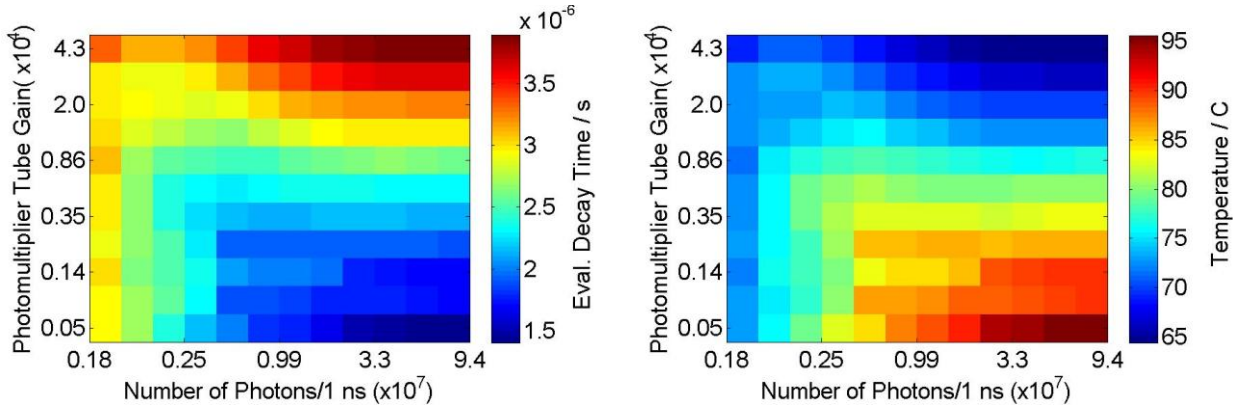

Figure 4.2: PMT in normal mode at T=100 °C, decay time (left) and evaluated temperature (right).

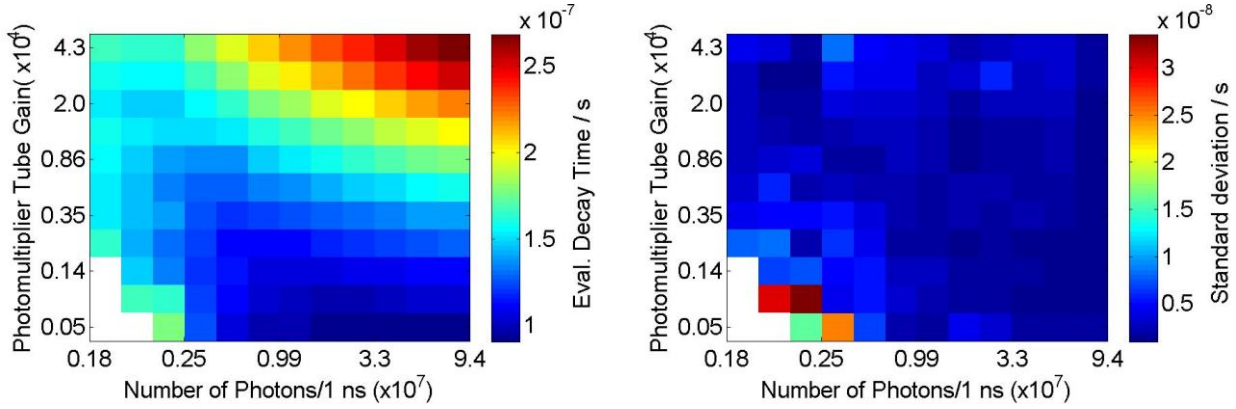

Figure 4.3: PMT in normal mode at T=181 °C, decay time (left) and standard deviation (right).

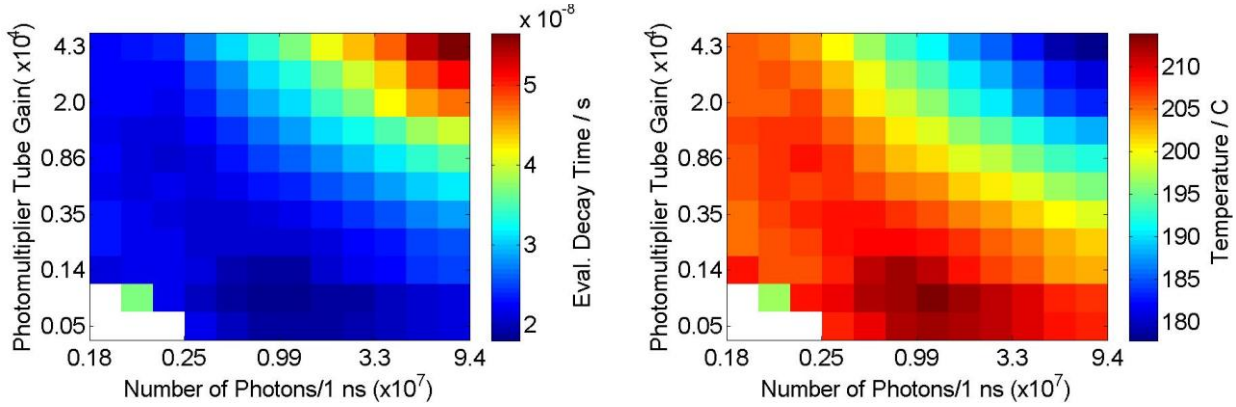

Figure 4.4: PMT in normal mode at T=246 °C, decay time (left) and evaluated temperature (right).

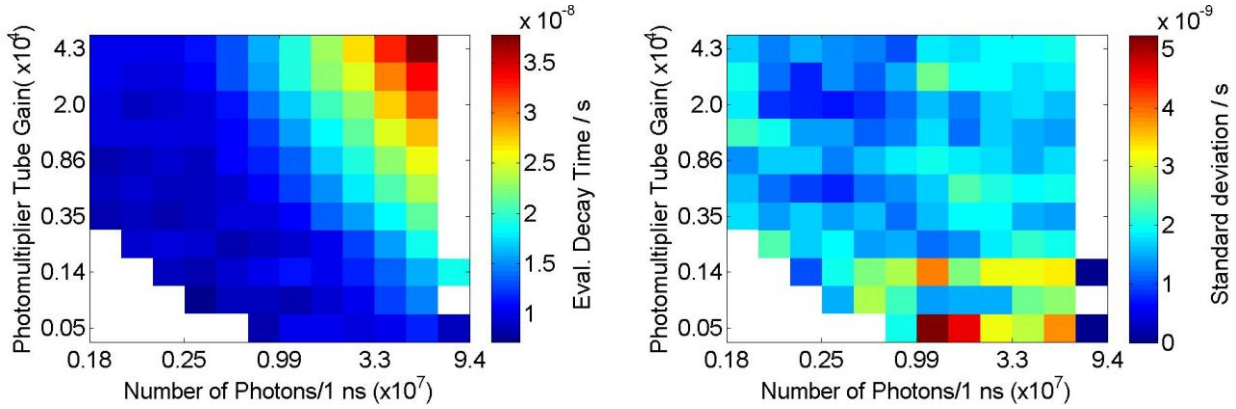

Figure 4.5: PMT in normal mode at T=288 °C, decay time (left) and standard deviation (right).

The PMT saturation is evident at high gain and high intensity (Upper right corner of the matrix) as illustrated by figures 4.1- 4.5. The saturation manifests itself on the decay time by increasing the decay time in areas of saturation. Saturation exists in all of the matrices ranging from room temperature up to the highest temperature. PMT also have demonstrated areas of linear response at low gain and extending over a photon count range (0.25-9.4) $\times 10^7$.
As temperature increases the phosphorescence intensity gets weaker that leads to empty matrix elements at regions of low gain and low number of photons as shown in figures 4.4- 4.5. The empty cells are filled with white color in order to be distinguished more easily. Also at higher temperatures, empty cells occur at the highest number of photons. This occurs because the maximum laser excitation energy per pulse is held constant but the phosphorescence gets weaker as temperature increased.
Since the value of the computed temperature is directly related to the phosphorescence decay time, saturation influences the value of the evaluated temperature as seen in figure 4.2. The evaluated temperature values spread over a span of 65-95 °C. Saturation yields longer decay times, which is translated as lower temperature. The fact that all of the matrix elements are measured at the same temperature indicates that the temperature gradient visible is resulting from the saturation effect on the decay time and consequently the evaluated temperature. At higher temperature, as the linear mode region extends the temperature is stable in larger areas than that produced at lower temperatures.
The phosphorescence signal voltage registered by the PMT detector is shown in figure 4.1. By relating the decay time matrix to the phosphorescence signal peak intensity, saturation can be avoided for each gain. The artifact appearing at the left side of the matrix is of unidentified nature. This nonlinear effect appears to be only affected by the number of incident photon, while the gain change seems to have no effect on this nonlinear behavior. This artifact is visible in all of the detectors' matrices.

4.1.2 Amplified PMT mode

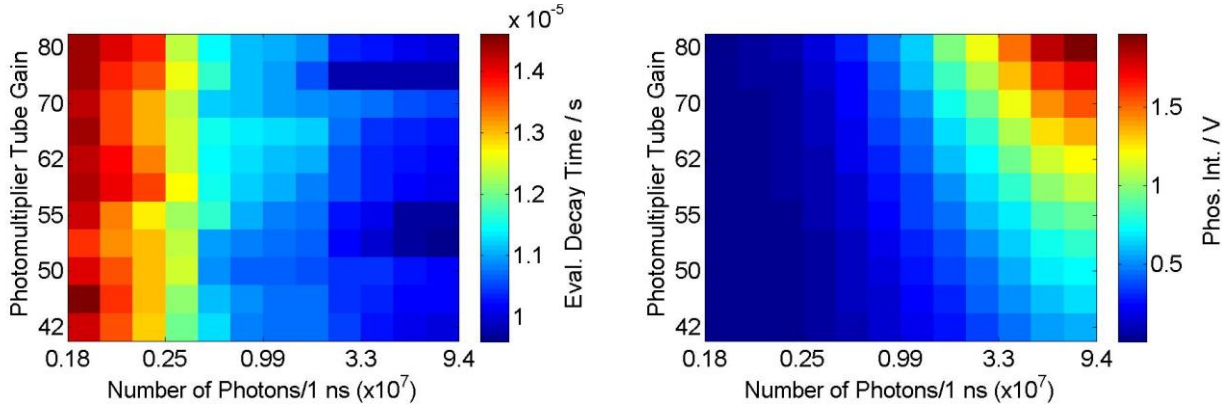

Figure 4.6: PMT in Amplified mode at *T*=21 °C, decay time (left) and phosphorescence intensity (right).

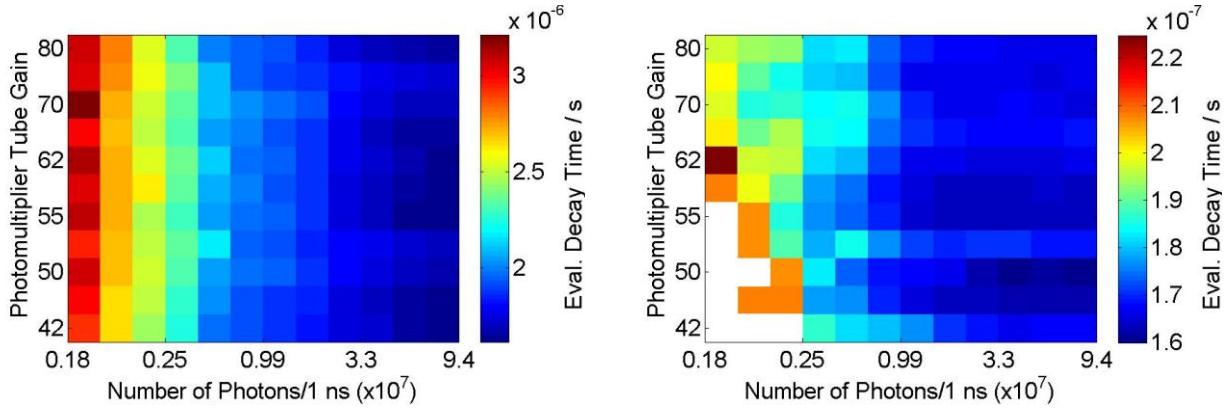

Figure 4.7: PMT in Amplified mode at (left) *T*=100 °C decay time, (right) T=181 °C decay time.

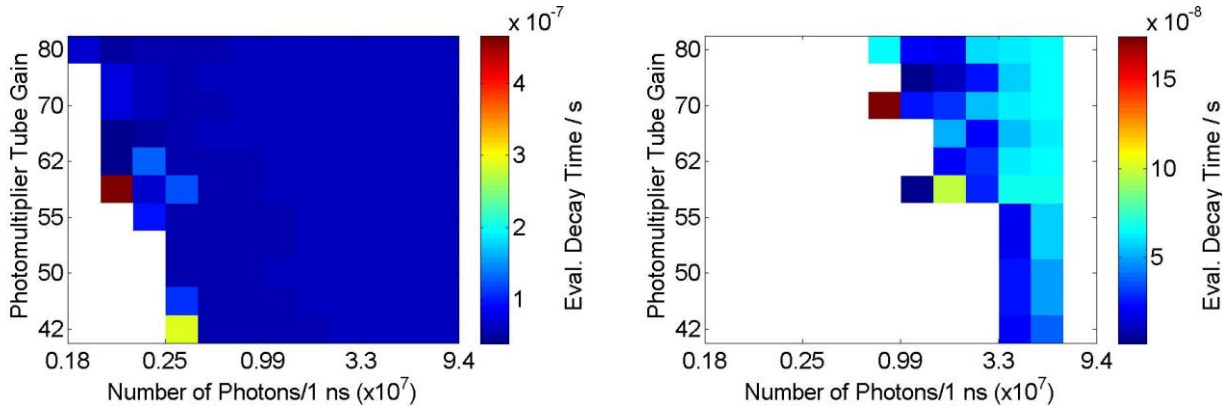

Figure 4.8: PMT in Amplified mode at (left) *T*=246 °C decay time, (right) T=288 °C decay time.

The PMT running in amplified mode of operation shows a larger area of linearity compared to the normal mode of operation. This is because using a current to voltage amplifier permits driving the PMT at much lower gain. Driving the PMT at lower gains in the amplified mode of operation provides a wider area of linear operation of the detector. The amplified PMT gain range extends from 40 to 80. This is very limited compared to the gain range when the same PMT is driven in normal mode (480 - 42500). What the amplified PMT lacks in the internal gain is compensated by the amplification factor of the current to voltage amplifier. The amplification factor of the amplifier is 1200 (derived earlier in section 3.2.5).

Although the amplifier puts the PMT in a stable linear region of operation, the used amplifier suffers from low bandwidth. The low bandwidth inflects a broadening to the amplified signal. This amplifier has a bandwidth of 5 MHz that is 200 ns time-scale broadening to the generated signal. This broadening limits the operational range of the PMT to decay times greater than 200 ns. The broadening effect produced buy amplifier affects the evaluated decay times faster than 200 ns because the fitting routine possibly fits part of the broadening slope instead of the actual phosphorescence decay. With even faster decay times, the exponential decay merges with the broadened peak and thus renders them undistinguishable. This is evident in figure 4.8 for 246 °C temperature where the decay time matrix loses its resolution and decay time gradient. This

broadening problem can be solved by deploying a high bandwidth amplifier. Compared to normal PMT mode the amplified PMT has greater number of lost cells at temperatures 246 and 288 °C. That means that unless a higher bandwidth amplifier is used, decay times faster than 200 ns could not be accurately evaluated.

4.2 Linearity response of a time-gated PMT: Hamamatsu H11526-20-NF

4.2.1 Time-gated PMT in continuous mode

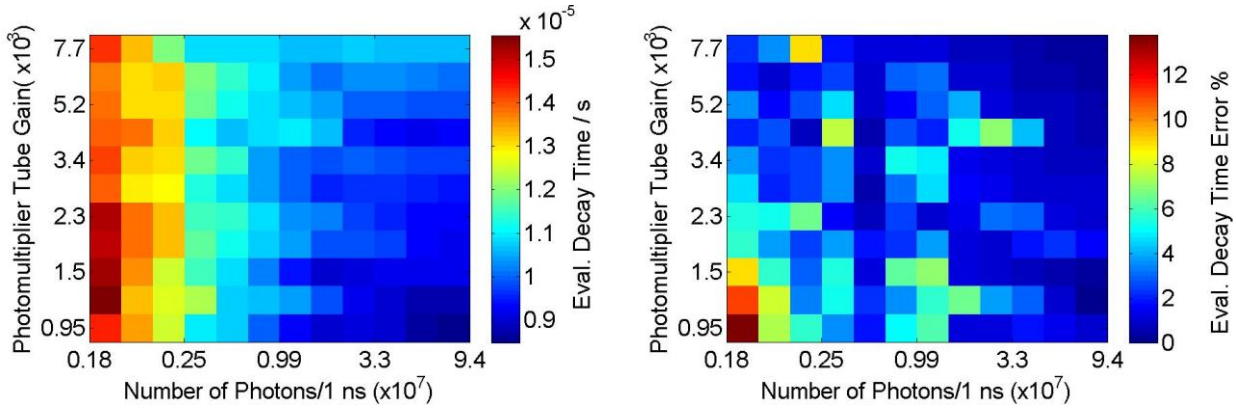

Figure 4.9: Time-gated PMT in continuous mode at T=21 °C, decay time (left) and percentage error (right).

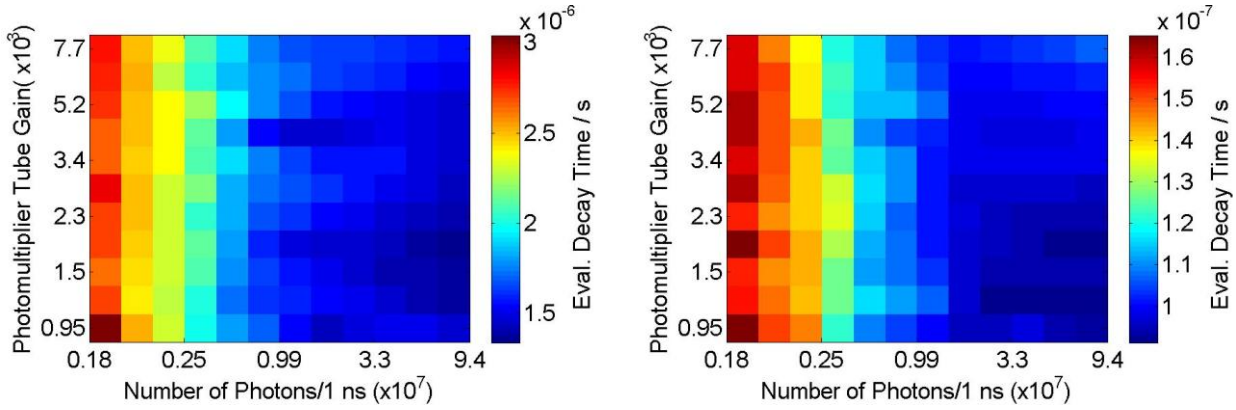

Figure 4.10: Time-gated PMT in continuous at (left) T=100 °C decay time, (right) T=181 °C decay time.

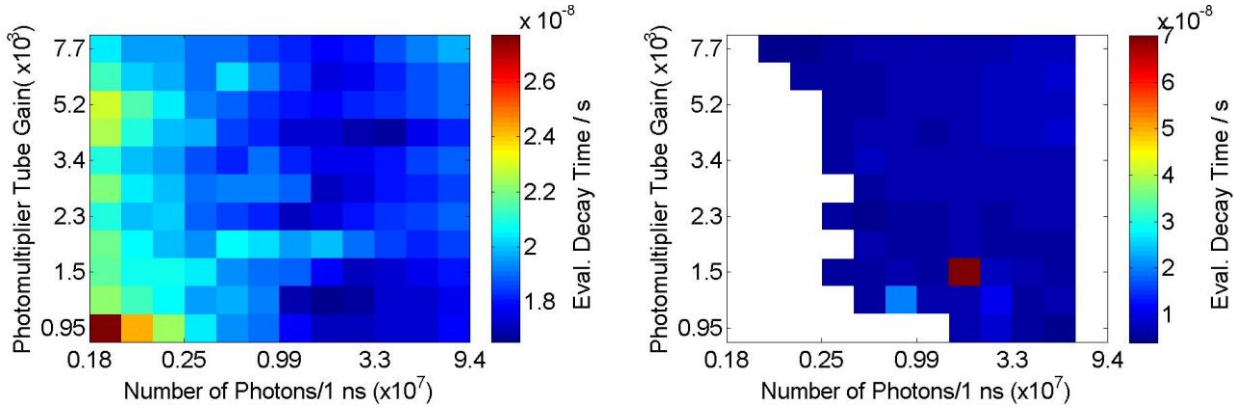

Figure 4.11: Time-gated PMT in continuous at (left) T=246 °C decay time, (right) T=288 °C decay time.

The time gated PMT operating in continuous mode displays a response matrix similar to the one seen with the amplified PMT. This is because the time gated PMT device has a luminous sensitivity that is almost a factor of 13 higher than the normal PMT. This indicates that in order to produce the same signal intensity level as the normal PMT, the time gated PMT is driven with much lower gain. The gain ranges of both detectors as listed in table 3.5 also verifies this. The time gated PMT region of linear operation is similar in distribution as the one for amplified PMT. The matrix element loss is only visible at the highest temperature (288 °C). The losses are located at the right side of the matrix due to phosphorescence intensity degradation at high temperatures. The other losses are at the left region of the response matrix.

It also displays the decay time gradient seen at the left edge of the response matrix. This artifact seems to disappear at a constant number of incident photons (around 0.25×10^7 photons/1ns) through the temperatures 21, 100, 181, and 246 °C.

4.2.2 Time-gated PMT in time-gated mode

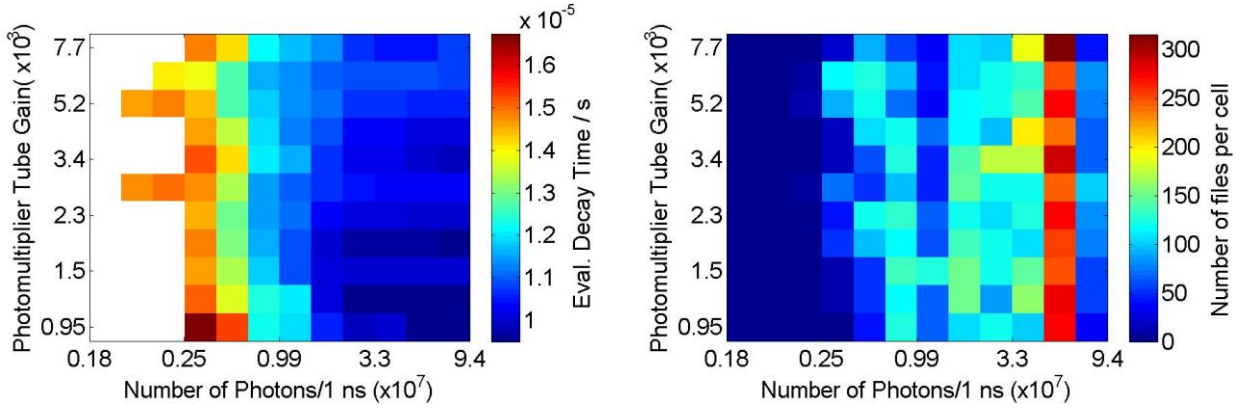

Figure 4.12: Time-gated PMT in gated mode at T=21 °C, decay time (left) and number of files per cell (right).

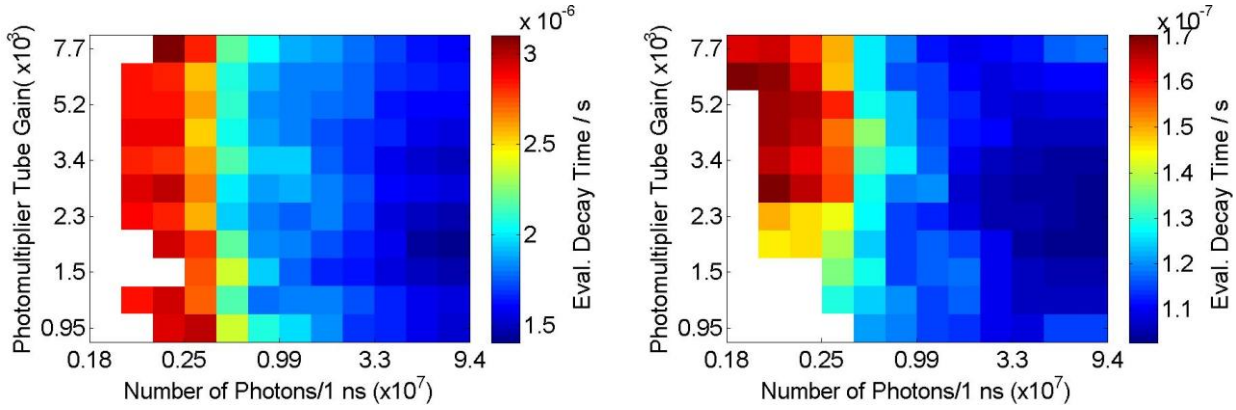

Figure 4.13: Time-gated PMT in gated at (left) *T*=100 °C decay time, (right) *T*=181 °C decay time.

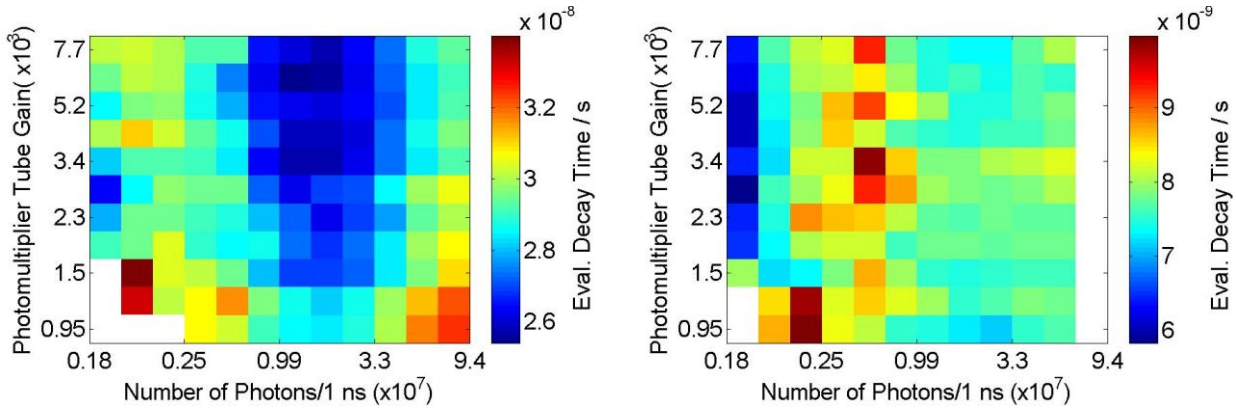

Figure 4.14: Time-gated PMT in gated at (left) *T*=246 °C decay time, (right) *T*=288 °C decay time.

When the time gated PMT is running in time-gated mode, it gives similar results to the continuous mode of operation except for the number of matrix element losses. The losses in the response matrix are due to the signal intensity loss due to gating. The matrix element losses are less at higher temperatures, which is related to the decreasing of the signal to noise criterion in the fitting code. This factor is decreased to recover decay curves with low signal intensity level. Otherwise the matrix of the high temperature would suffer from severe matrix elements losses.
The time-gated mode of this detector has a delay time of 180 ns. That indicates that the detector response is delayed 180 ns before the phosphorescence peak is shown. To compensate for this delay the trigger signal from the Nd:YAG laser is set to -150 ns instead of the default +20ns. The time gate applied is 1 ms in width and with time delay of 0.0 s from the q-switch triggering signal.

4.3 Linearity response of a MCP-PMT: Hamamatsu R5916U-50

4.3.1 MCP-PMT in normal mode

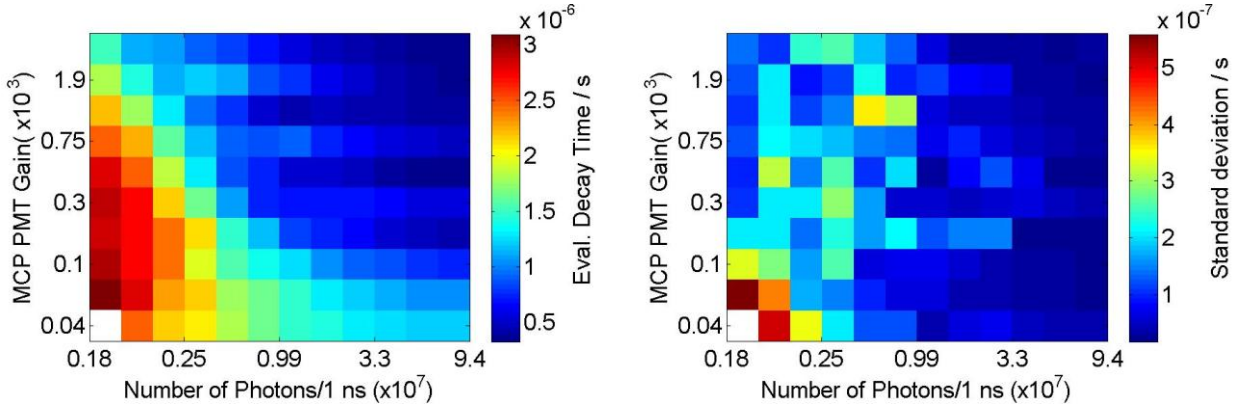

Figure 4.15: MCP PMT in normal mode at T=100 °C, decay time (left) and standard deviation (right).

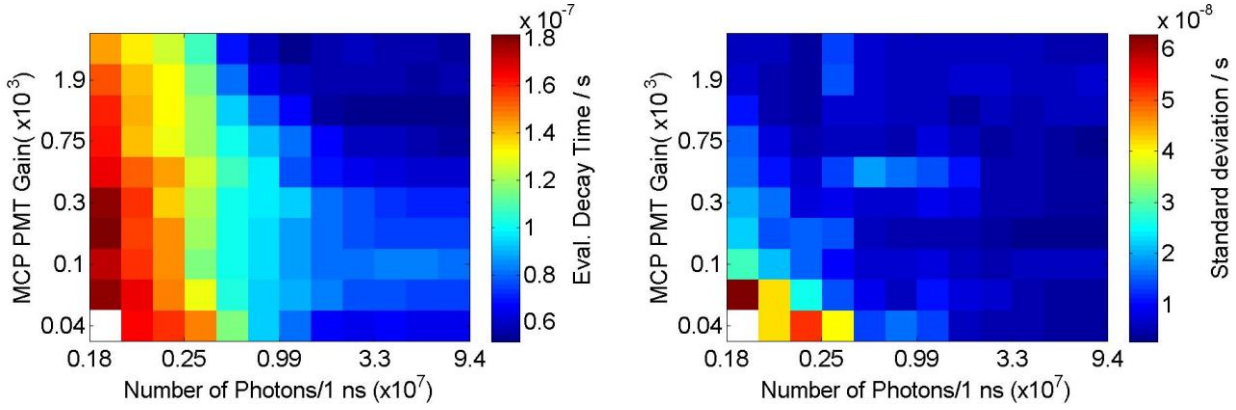

Figure 4.16: MCP PMT in normal mode at T=181 °C, decay time (left) and standard deviation (right).

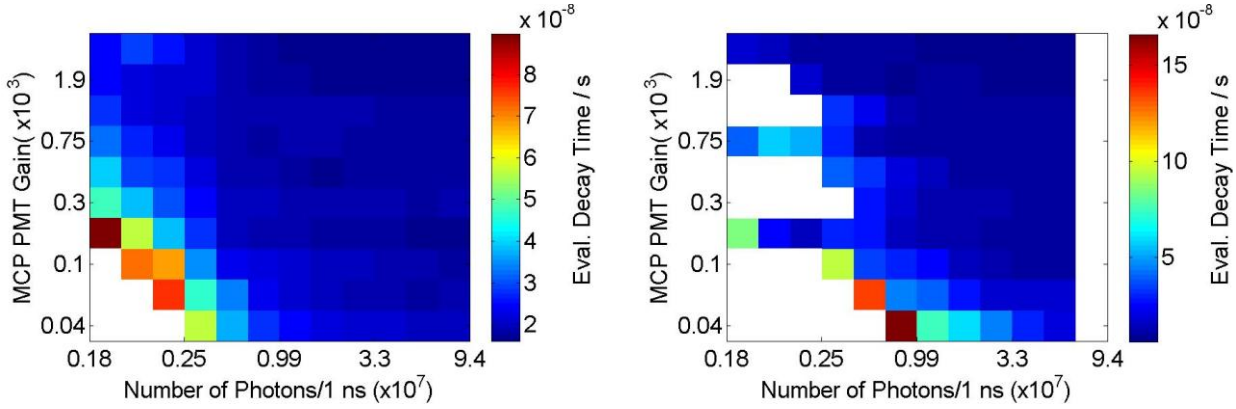

Figure 4.17: MCP PMT in normal mode at (left) T=246 °C decay time, (right) T=288 °C decay time.

The MCP PMT device is always used in gated mode, but the time gate can be moved to cover the whole phosphorescence signal. In this situation, the MCP PMT can be considered to be working in continuous mode. To be able to shift the time gate the trigger setting in the laser was changed to -75 ns. This value made the entire phosphorescence pulse visible and uncut by the time gate.
In addition, the MCP PMT forces a limitation on the length of the measured decay time because the maximum time gate width is 10 μs. This value translates as a minimum temperature detection of 100 °C for the $CdWO_4$ phosphor. For this reason, the first response matrix for the MCP PMT device starts at a temperature of 100 °C.
From the figures 4.15- 4.17 it can be noticed that the MCP PMT detector has its linear response region in the matrix elements located at high number of incident photons and detector gain. The saturation artifact visible in previously mentioned detector also manifest in the region at the left side of the MCP PMT response matrix. In the MCP-PMT, the artifact has a diagonal shape that is different from the other detectors. This means that this behavior is MCP-PMT specific.

4.3.2 MCP-PMT in time-gated mode

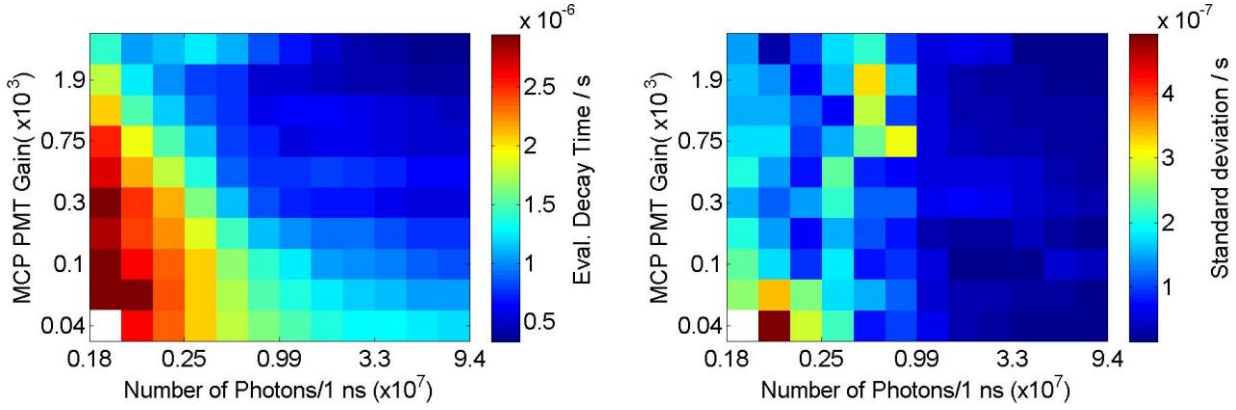

Figure 4.18: MCP PMT in gated mode at *T*=100 °C, decay time (left) and standard deviation (right).

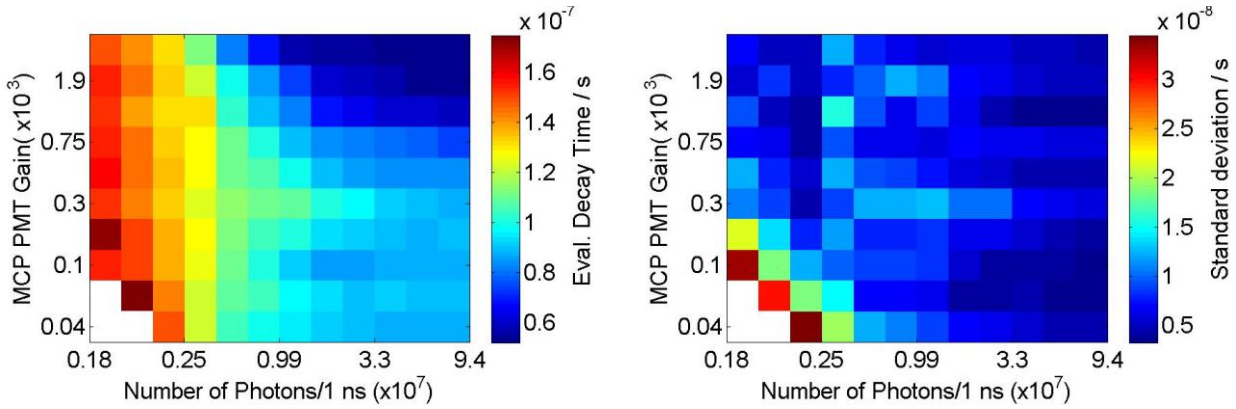

Figure 4.19: MCP PMT in gated mode at *T*=181 °C, decay time (left) and standard deviation (right).

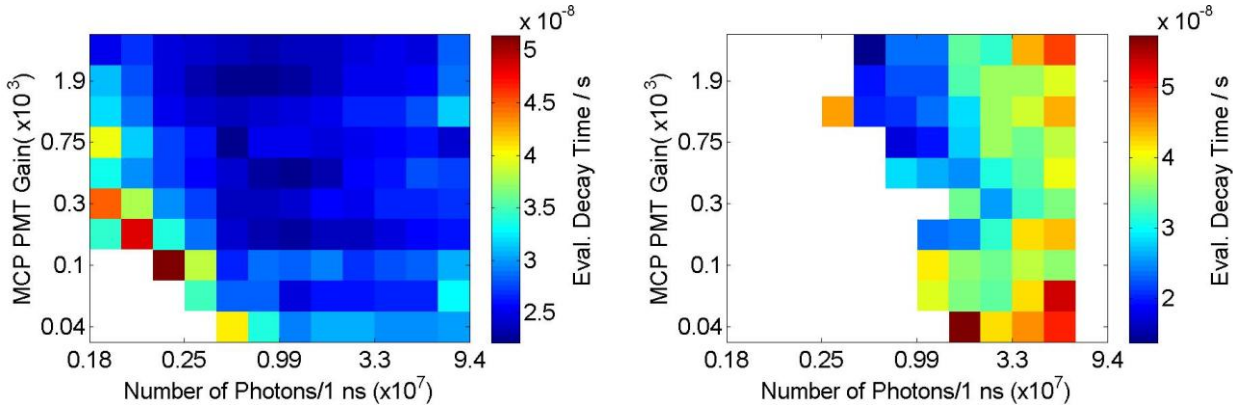

Figure 4.20: MCP PMT in gated mode at (left) *T*=246 °C decay time, (right) *T*=288 °C decay time.

Running the MCP PMT in gated mode yields similar plots as in the continuous mode. Matrix element losses at the highest temperature are substantial. Due to the fast transit time (1 ns) of the MCP PMT, the gating of the peak doesn't cause a time delay. Linear operation regions are seen at matrix cells that have high detector gain and high intensity. Also, the limitation of the time gate applies here which limited the minimum measurement temperature to 100 °C.

4.4 Linearity response of a APD: Hamamatsu Si-APD S5343

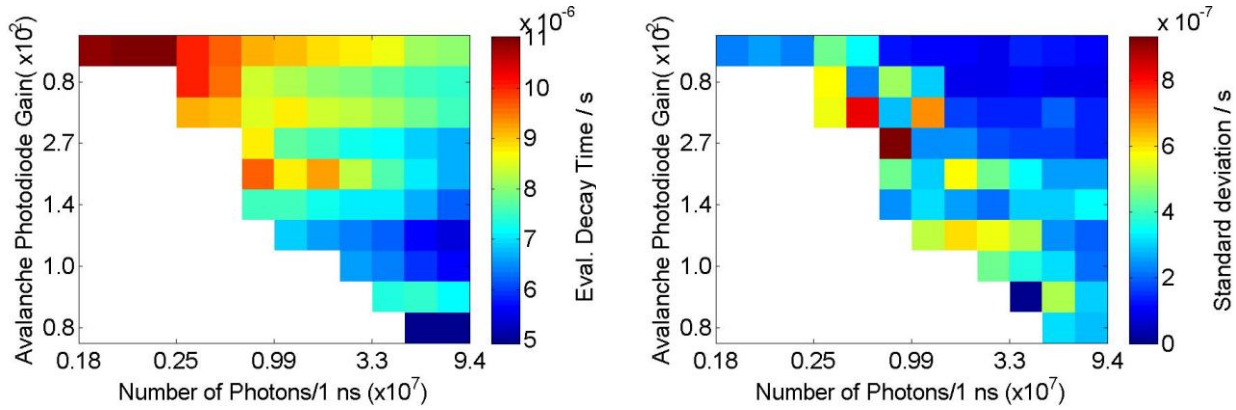

Figure 4.21: Avalanche photodiode at *T*=21 °C, decay time (left) and standard deviation (right).

The Si-avalanche photodiode has a break down voltage of 156 V, which meant that the maximum output signal level is limited. In addition, the APD suffers from limited gain range (60 - 470). This meant that the response matrices of the APD have empty cells at low intensities and low gain. The matrix cell loss increases with increasing temperature, rendering the APD response matrices at 246 and 288 °C unbeneficial. At the highest gain the saturation effects is highly visible because the APD was driven at reverse voltages close to the breakdown voltage. Regardless of the behavior seen at the highest gain the APD shows a region of linear operation that could be exploited using a high bandwidth amplifier.

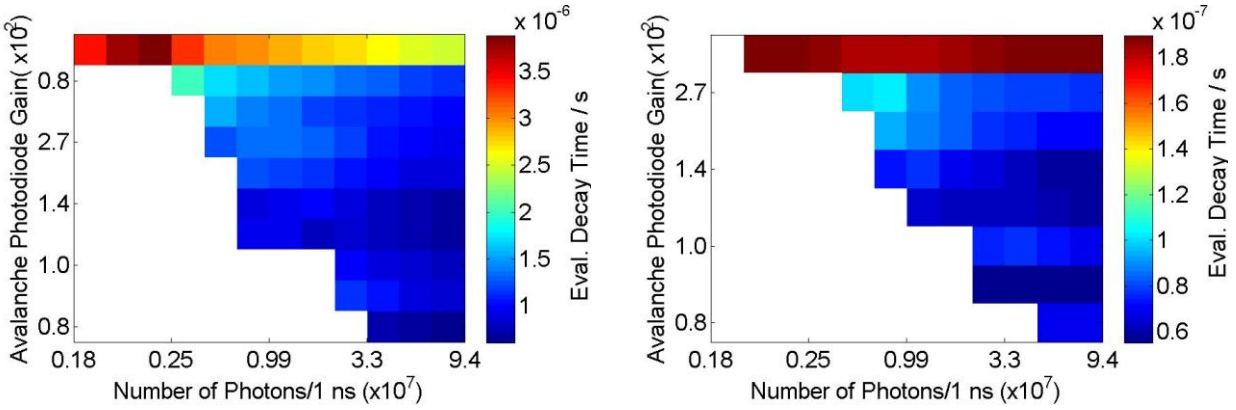

Figure 4.22: Avalanche photodiode at (left) *T*=100 °C decay time, (right) *T*=181 °C decay time.

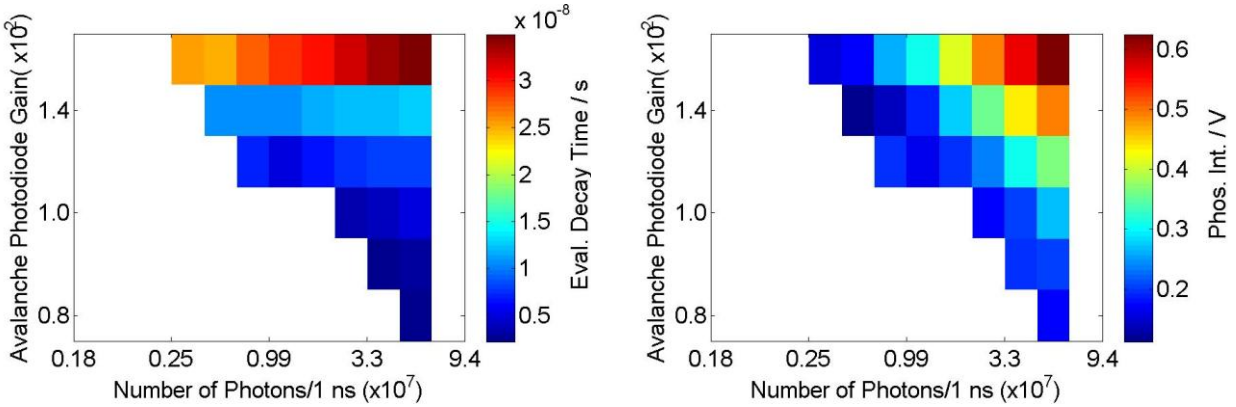

Figure 4.23: Avalanche photodiode at (left) *T*=246 °C decay time and Phosphorescence Intensity (right).

5. Discussion

The chapter presents comparison and characterization of the detector specific response matrices produced by different detectors operated under different modes of operation (amplified, time-gated). Explanation of detector nonlinear behavior at low incident phosphorescence level is attempted.

5.1 Detector comparison: APD, PMT, time-gated PMT (Continuous mode), MCP-PMT (Continuous mode)

This sub-chapter discusses the detector running under normal mode of operation i.e. running without external amplifier or time gating. A comparison is built for all of the detectors at measurement temperature of 100 °C and represented in figure 5.1.

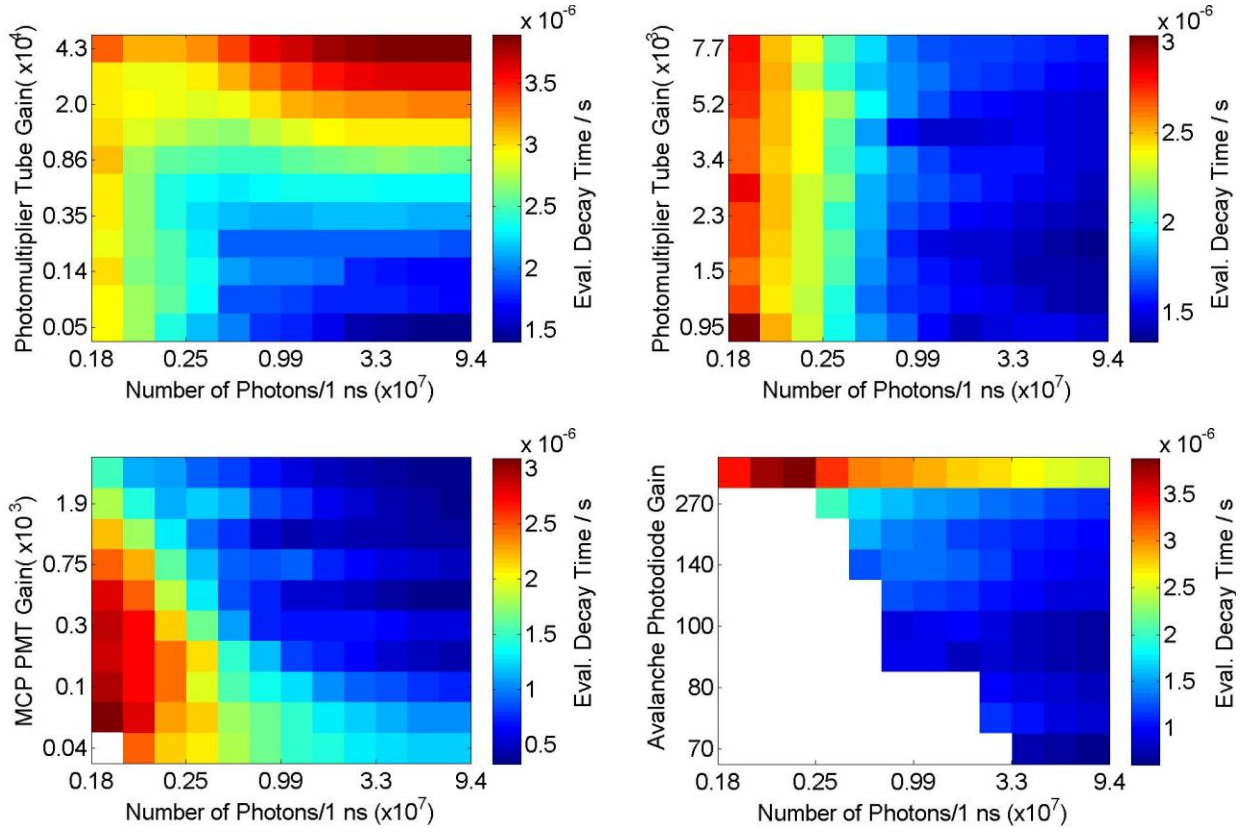

Figure 5.1: Decay time vs. detector gain and number of incident photons at a measurement temperature of 100 °C. *Top left:* PMT, *top right:* time-gated PMT, *bottom left:* MCP-PMT, *bottom right:* APD.

The detectors are subjected for similar experimental conditions. The measurements are done at a temperature of 100 °C with an individual deviation of 0.5 degrees from the assigned temperature. Before the matrix measurement was started, the temperature stability was checked with achieved standard deviation of thermocouple temperature of 0.1 °C within the last 2 minutes.

The PMT experiences nonlinear response at regions of high gain and high intensities, while linearity is achieved at regions of low input light levels and low gain. Time-gated PMT provides

a greater linear response regions compared to the normal PMT. The MCP-PMT shows regions of linear mode of operation at areas of high intensities and high gain. The linear behavior of the MCP-PMT is opposite to that of the normal PMT. This behavior could be contributed to the fact that the MCP-PMT has a rated maximum output current of 350 mA, while the PMT is limited to 100 µA maximum output current. This means that the conditions that drive the normal PMT into nonlinear behavior do not affect the linearity of the MCP. The fact that the MCP-PMT has a maximum time gate of 10 µs limits the use of the MCP for slower decay times. The MCP-PMT was designed to detect picoseconds pulses, so a time gate of 10µs is more than enough for that purpose. APD shows a linear behavior in almost the whole matrix cells. The nonlinearity of the APD at the highest gain is due to the fact that the APD is ran at reverse voltage close to the breakdown voltage, and thus experiences saturation. The APD matrix has almost half of it cells lost because of the limitations of APD gain range.

The evaluated decay time range for the PMT and time gated PMT is almost identical. The mean evaluated decay time in the linear response regions of the normal PMT and the time gated PMT are close to each other, 1.7 µs and 1.5 µs respectively. The APD shows a mean decay time of around 1.0 µs in regions of linear behavior. The lowest mean decay time is provided by the MCP-PMT with decay time values around 0.5 µs. The evaluated decay time is almost half of that produced by the APD and one third of those produced by the normal PMT and the time-gated PMT. Further detailed study of the impact of the detector-generated standard deviation on the evaluated decay time is presented in figure 5.2.

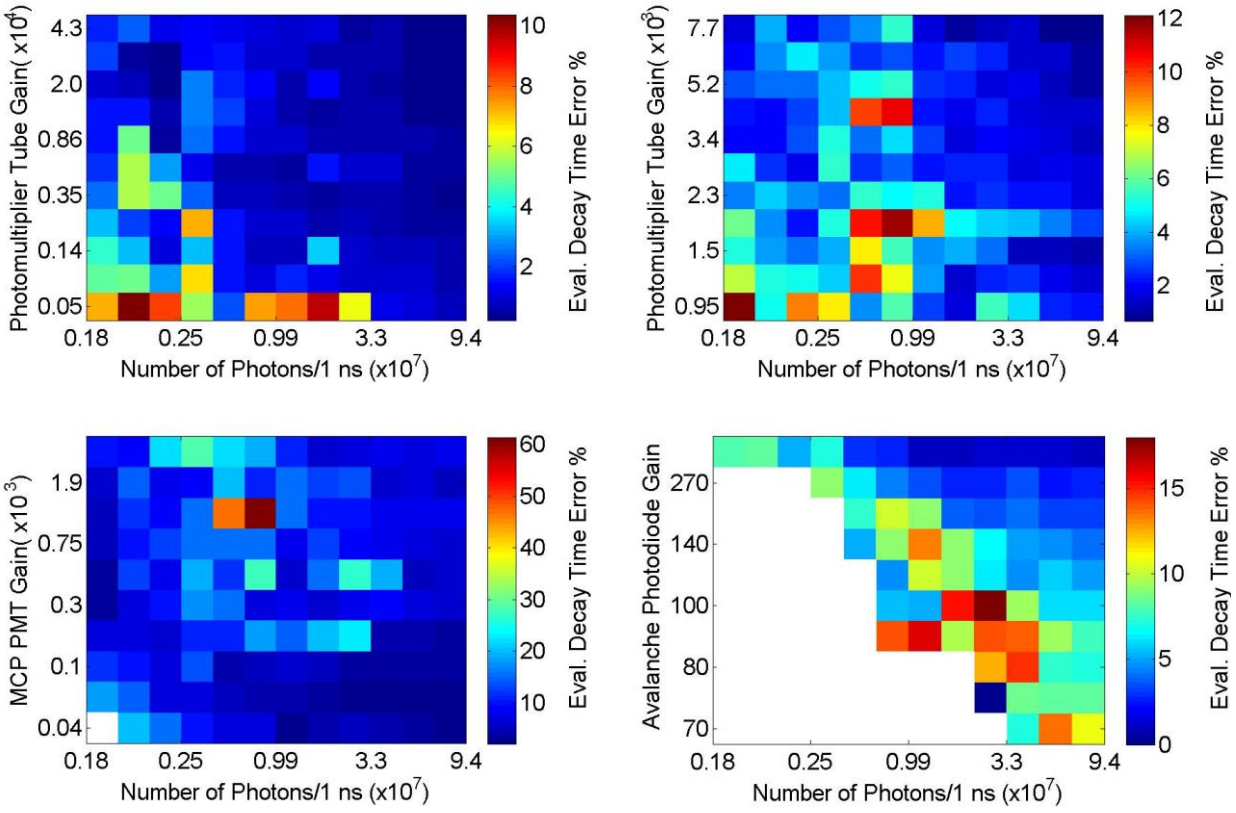

Figure 5.2: Decay time percentage error vs. detector gain and number of incident photons at a measurement temperature of 100 °C. *Top left:* PMT, *top right:* time-gated PMT, *bottom left:* MCP-PMT, *bottom right:* APD.

Minimum error in the evaluated decay time is found in the response matrices of the normal PMT and time-gated PMT. The error is low in cells with high signal to noise ratio and it increases as the matrix extends towards areas of less phosphorescence intensity and lower gain. All of the detectors have almost the same percentage error range. The outburst of the percentage error bar in MCP-PMT is due to the high error presented by only two cells. The reset of the error distribution varies between 2 % to 15 %.

A particular pattern evident in all of the detectors is the rise of the decay time at the lower intensities. The number of incident photons, or in other words, the phosphorescence intensity affects this behavior. The gain effect is minimum compared to the effect introduced by the phosphorescence intensity. There are two explanations to this phenomenon presented by two articles [22, 29]. The first article [22] indicates that at low intensity levels the photomultiplier tube showed a nonlinear behavior as in the case of high intensity levels. The second article [29] states that the decay time decreases with increasing exciting laser pulse energy. Although, the article used another phosphor in the investigation, the phosphor showed slower decay times at lower laser pulse energies. This phenomenon could be a result of the combination of both effects, the detector nonlinearity at low input intensity levels and to slower decay times at low laser pulse energy. In order to visualize the effect of laser pulse energy on the evaluated decay time, the decay time is plotted against the laser pulse energy (figure 5.3).

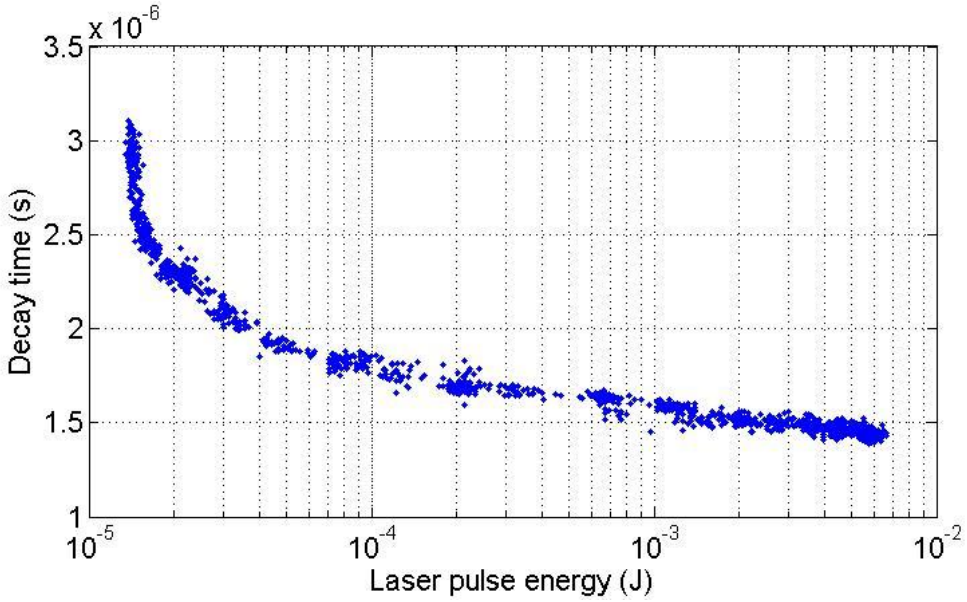

Figure 5.3: Decay time vs. laser pulse energy for time-gated PMT at temperature of 100 °C and gain 2800.

From figure 5.3 it can be seen that decay time value increases with decreasing laser energy as mentioned in the article. The factor by which the decay time increases as factor of laser pulse energy reduction is almost the double. The decay time at the highest laser pulse energy is about 1.5 μs compared to 3.0 μs at the lowest laser pulse energy.

The increase of the decay time is caused by the deformation of the phosphorescence decay curve when the laser intensity is changed. This effect is visualized when the phosphorescence intensity at the start of the fitting window is divided by the peak phosphorescence intensity of the decay. In theory, a constant decay time should produce a constant ratio. Any change in the ratio should be detected as a change in the evaluated decay time as shown in figure 5.4.

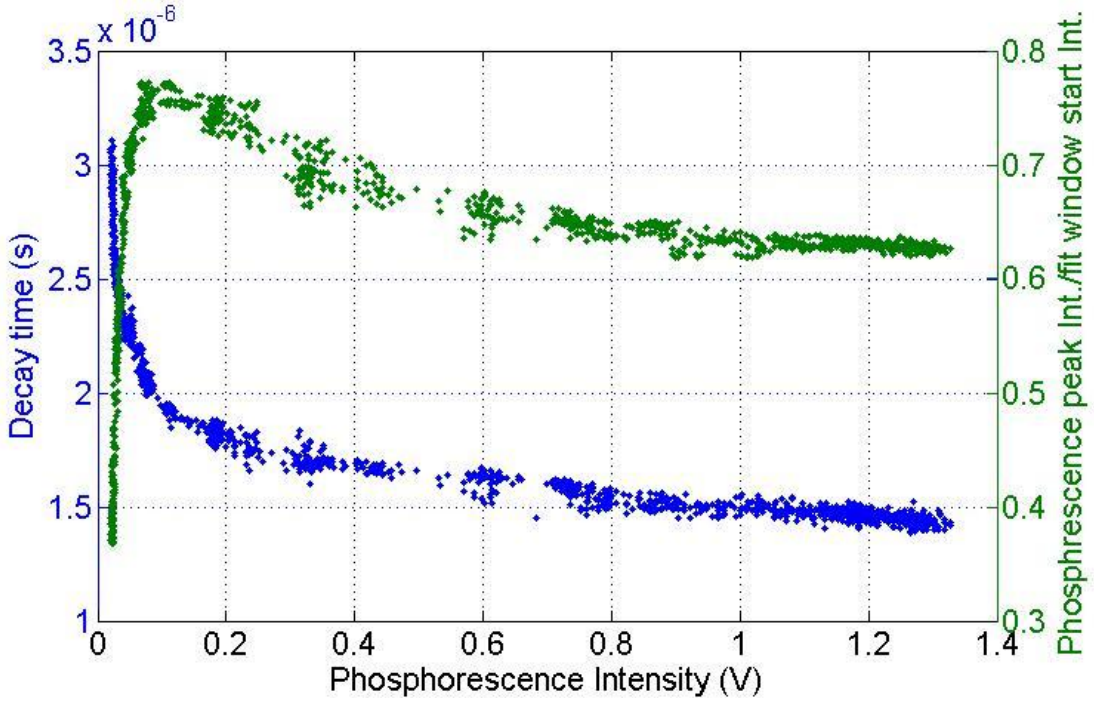

Figure 5.4: Ratio of start of fit window Intensity and peak phosphorescence intensity (right), decay time (left), as function of phosphorescence intensity for time-gated PMT at temperature of 100 °C and gain 2800.

The deviation of ratio indicates a change in the profile of the phosphorescence decay. This change in the phosphorescence decay profile could be either due to nonlinearity produced by the detector, or by a change of the phosphorescence emission properties. The change of the evaluated time is evident regardless of the effects causing it. The causes are narrowed to two possibilities that could cause the decay time deviation that either can act individually or combined.

The same comparison built in figure 5.1 at 100 °C is built again for measurement temperature of 246 °C in figure 5.5. The purpose of this comparison is to study the effect of the phosphorescence intensity on detector nonlinearity at high temperature. From figure 5.5, it can be directly noticed that regions of linear operation of all detectors have extended. This is because at higher temperatures the phosphor quantum efficiency drops. The drop of phosphor quantum efficiency means that the phosphor emits lower radiation with the same laser pulse energy used at the lower temperatures. Lower phosphorescence intensity cause the extension of the linear mode of operation of the detectors compared.

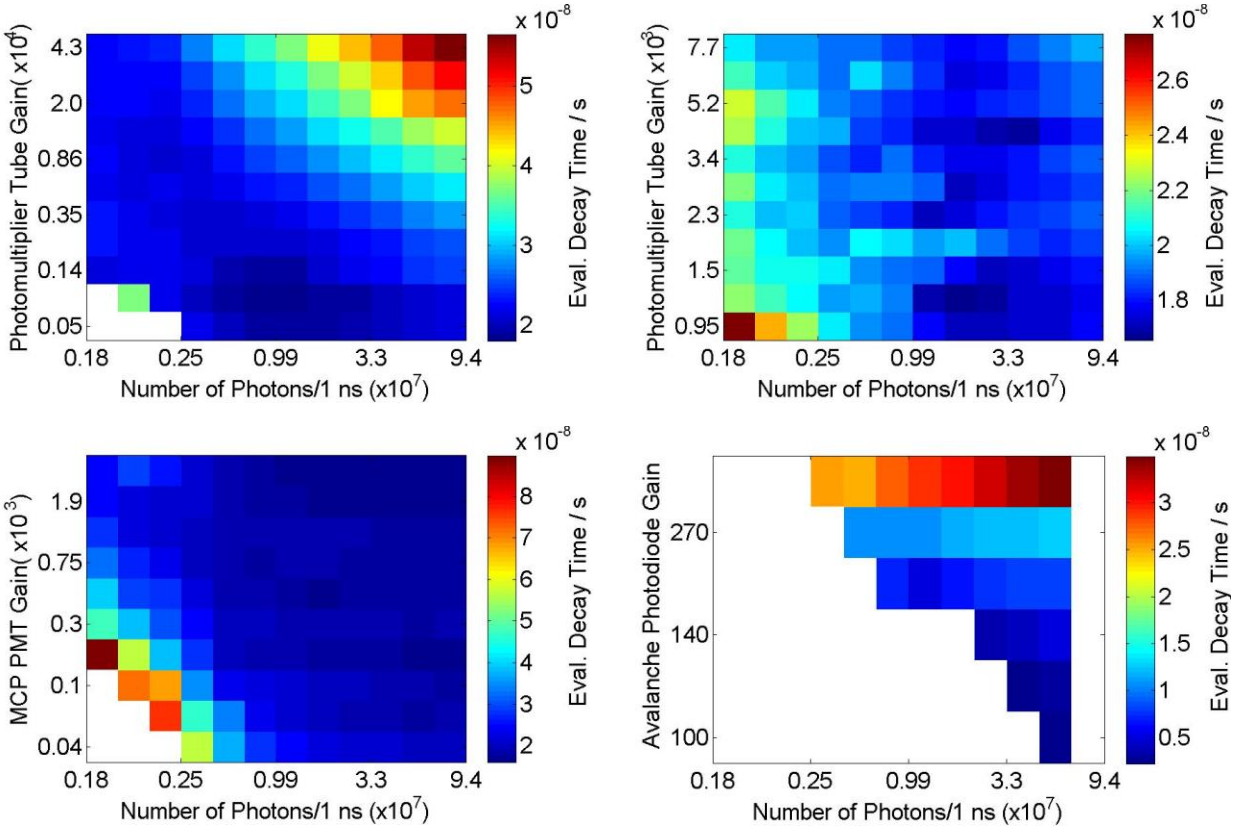

Figure 5.5: Decay time vs. detector gain and number of incident photons at a measurement temperature of 246 °C. *Top left:* PMT, *top right:* time-gated PMT, *bottom left:* MCP-PMT, *bottom right:* APD.

Higher temperatures yield lower phosphorescence intensity and since the noise level is almost constant, that leads into lower signal to noise ratio. The decrease of the signal to noise ratio increases the percentage error of the evaluated decay time. The APD measurement matrix at high temperatures is useless and do not provide beneficial data because only small fraction of the matrix shows decay time results.

5.2 Time-gated Devices

This sub-chapter compares the time gated PMT and the MCP-PMT individually as they run under the time gated function or continuously. Then the two detectors are brought to comparison between their time-gated modes of operation.

5.2.1 Time-gated PMT comparison: continuous mode vs. time-gated mode

The time gated PMT has the ability to be operated in two modes of operations, continuous and time-gated. Response matrices of both modes of operations are built and presented in figure 5.6. Time gating a signal can improve detection in cases where a lot of interfering radiation exists in the measurement environment that could go through to the detector. In this case, the detector can be set to operate in a small time-window (ns-ms) that minimizes the noise and improves detection capability.

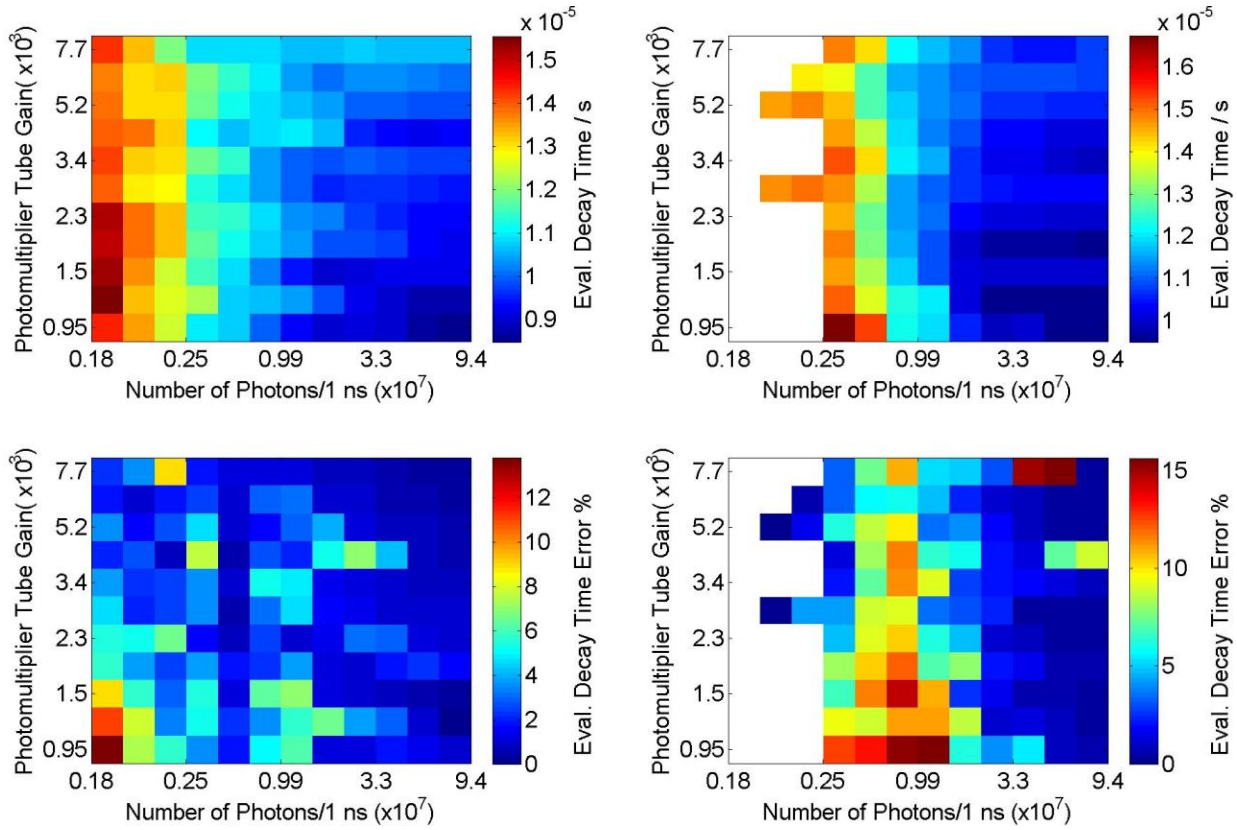

Figure 5.6: Decay time vs. detector gain and number of incident photons at a measurement temperature of 21 °C. *Left:* time-gated PMT continuous mode decay time and percentage error (below), *right:* time-gated PMT time-gated mode decay time and percentage error (below).

Regarding to evaluated decay time, both operation modes produces similar range of decay times with similar regions of linear detector operation. The time-gated mode suffers from matrix cell losses even at the lowest temperature. These losses are related to the time gating of the phosphorescence pulse, which reduces the final phosphorescence signal intensity. In theory, the gating mode allows the elimination of the intense peak that comes before the phosphorescence.

Then, the detector gain can be raised to compensate for the losses caused by time gating the signal. However, for the sake of comparison, the detector was held at the same conditions (gain, laser pulse energy) during matrix measurement. The percentage error of the decay time is higher in the time-gated mode than in the continuous mode. As mentioned, the signal-to-noise ratio drops in the time-gate mode which results in an increase in the percentage error of the decay time.

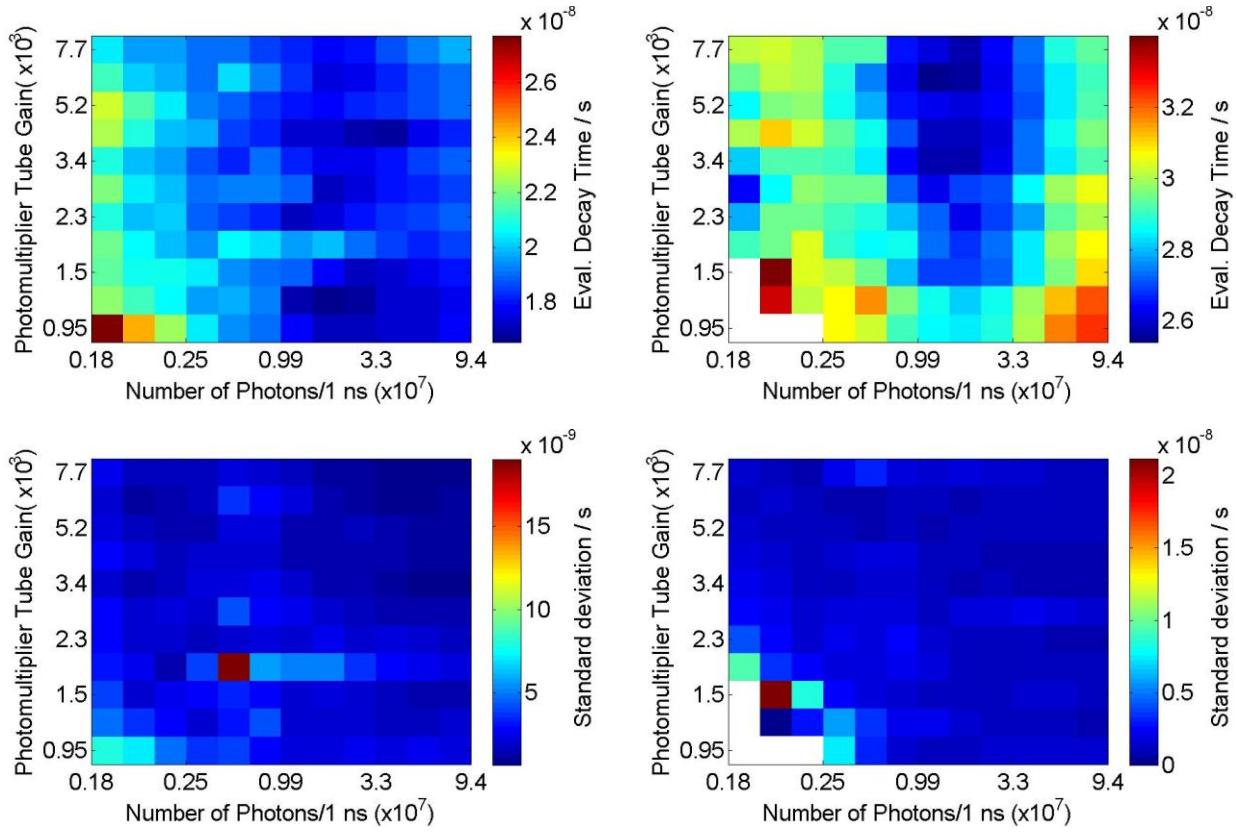

Figure 5.7: Decay time vs. detector gain and number of incident photons at a measurement temperature of 246 °C. *Left:* time-gated PMT continuous mode decay time and standard deviation (below), *right:* time-gated PMT time-gated mode decay time and standard deviation (below).

At temperature of 246 °C, the continuous mode of operation produces faster decay times than those produced by the time-gated mode. The standard deviation of the evaluated decay time lies in an identical range for both of the detector modes. The increase of the decay time values in the time-gated mode is related to the low phosphorescence intensity. The time-gating of the signal results in the reduction of the signal intensity because part of the decay peak is eliminated by the time gate. This results in the fitting of slightly slower phosphorescence decay because a part of the fast decay has been eliminated by the time-gate. At high temperatures, the decay times become faster and the time gate have more influence on the phosphorescence intensity after gating.

5.2.2 MCP-PMT comparison: continuous mode vs. time-gated mode

The MCP-PMT is characterized by its fast response and higher maximum output current compared other detectors. The continuous mode in MCP-PMT is achieved by extending the gate window over the whole phosphorescence decay. The time gate width was set to 10μs, the maximum time gate width possible.

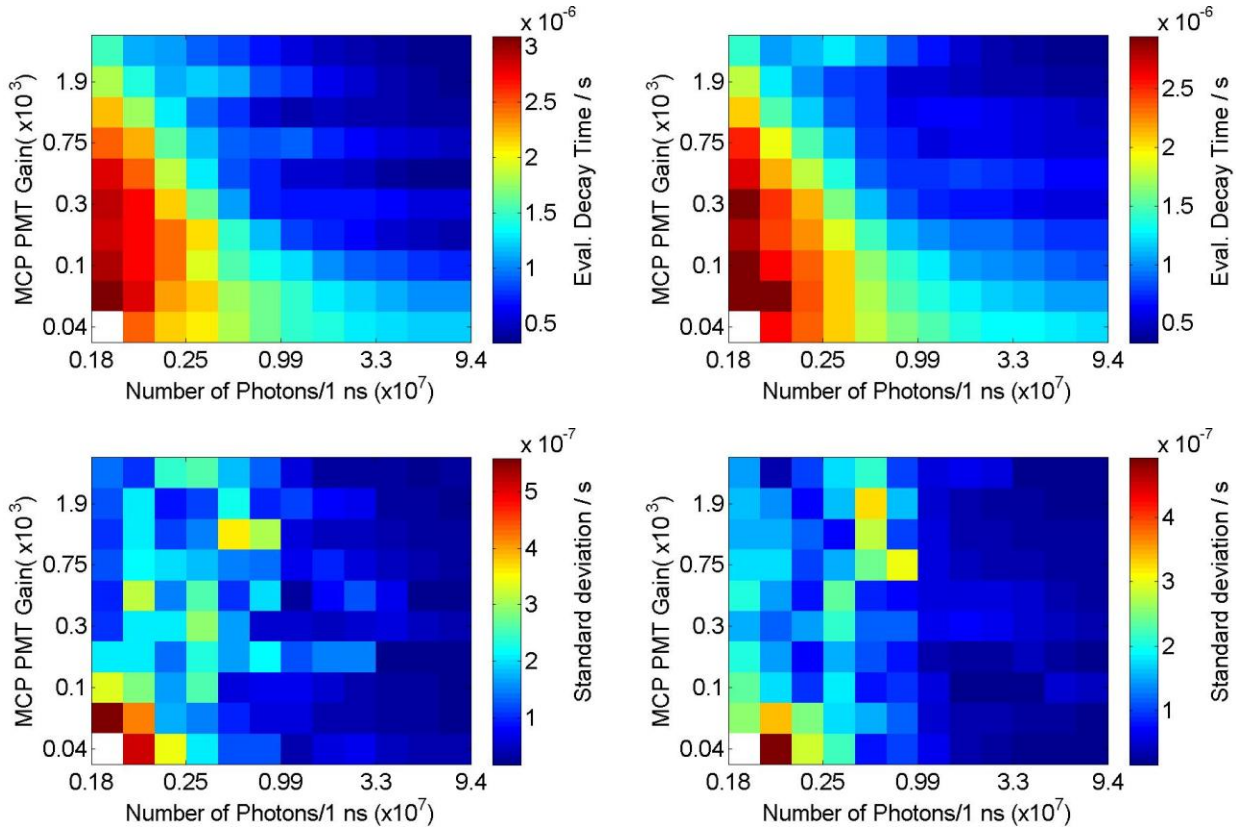

Figure 5.8: Decay time vs. detector gain and number of incident photons at a measurement temperature of 100 °C. *Left:* MCP-PMT continuous mode decay time and standard deviation (below), *right:* MCP-PMT time-gated mode decay time and standard deviation (below).

There are no noticeable differences between the continuous and time-gated modes regarding the evaluated decay time (figure 5.8). In addition, the standard deviation of the evaluated decay time falls in the same range (0.1μs-0.5μs) for both modes of operation. The decay time range is between 0.5 μs to 3 μs which correspond to a evaluated temperature span of 130-80 °C respectively at measurement temperature of 100 °C. The regions of linear operation of the two modes are located at almost the same location. The MCP-PMT shows minor differences between the gated and continuous modes of operation.

At higher temperature (246 °C), the behavior of both modes relating to decay times changes (figure 5.9). The time-gated mode displays slower mean decay time of 25 ns, while the continuous mode has a mean decay time of 20ns. The time-gated mode shows a higher standard deviation value of 5ns compared to 2ns produced by the continuous mode. These differences can be a result of the weaker phosphorescence at higher temperature and increased influence of the time gate on phosphorescence intensity reduction.

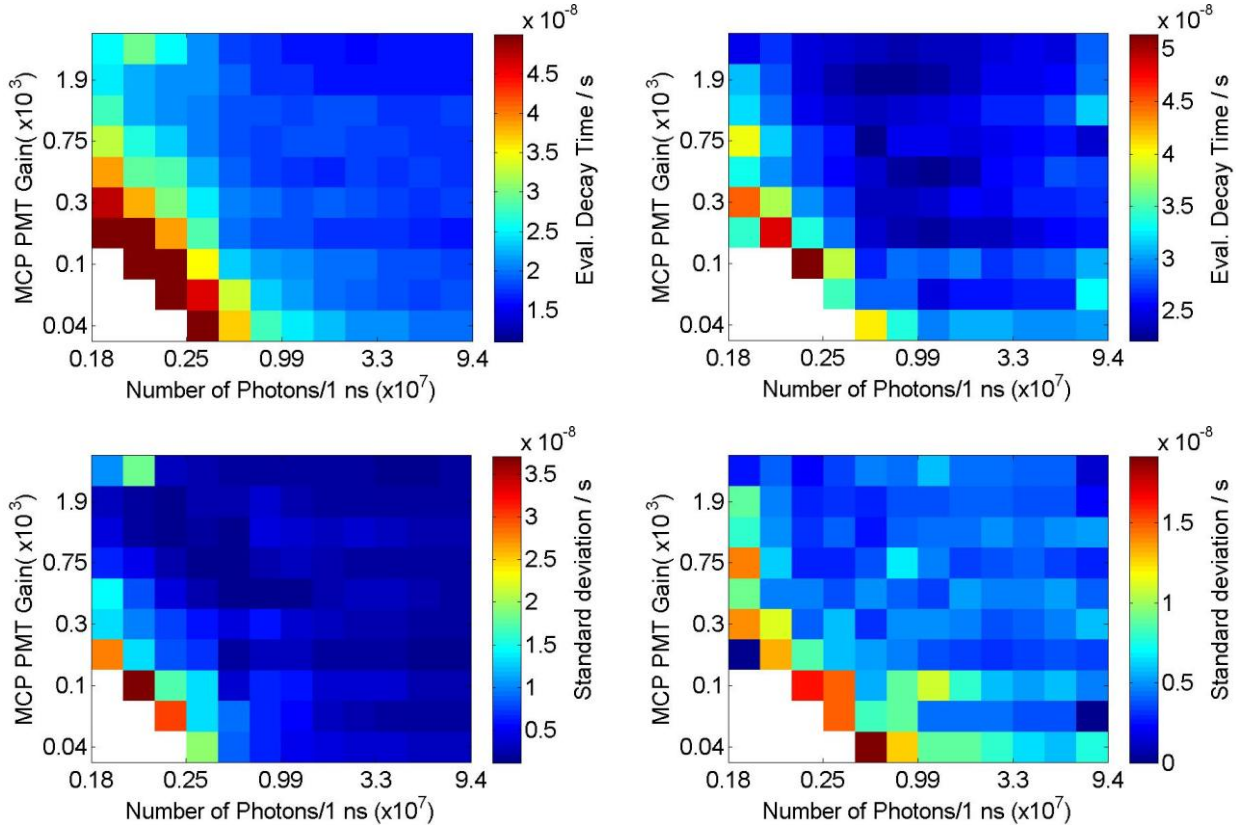

Figure 5.9: Decay time vs. detector gain and number of incident photons at a measurement temperature of 246 °C. *Left:* MCP-PMT continuous mode decay time and standard deviation (below), *right:* MCP-PMT time-gated mode decay time and standard deviation (below).

5.2.3 MCP-PMT vs. time-gated PMT comparison: time-gated mode

The MCP-PMT and time-gated PMT are two different detectors that have time gating capability. Comparison between the time-gated modes of the two detectors is performed in this section. On paper, the MCP-PMT is superior to the time-gated PMT by having large maximum output current (350 mA). However, the time-gated PMT has a time gate width that extends to DC compared to maximum gate width of 10μs for the MCP-PMT. Both detectors show the same range of decay times, but the regions of linear operation differ. The time gated PMT has regions of linear operation at cells that lie higher than 0.99×10^7 photon counts and for all gains. The MCP-PMT's region of linear response is extending over cells with high intensity low gain and lower intensity with increasing gain.

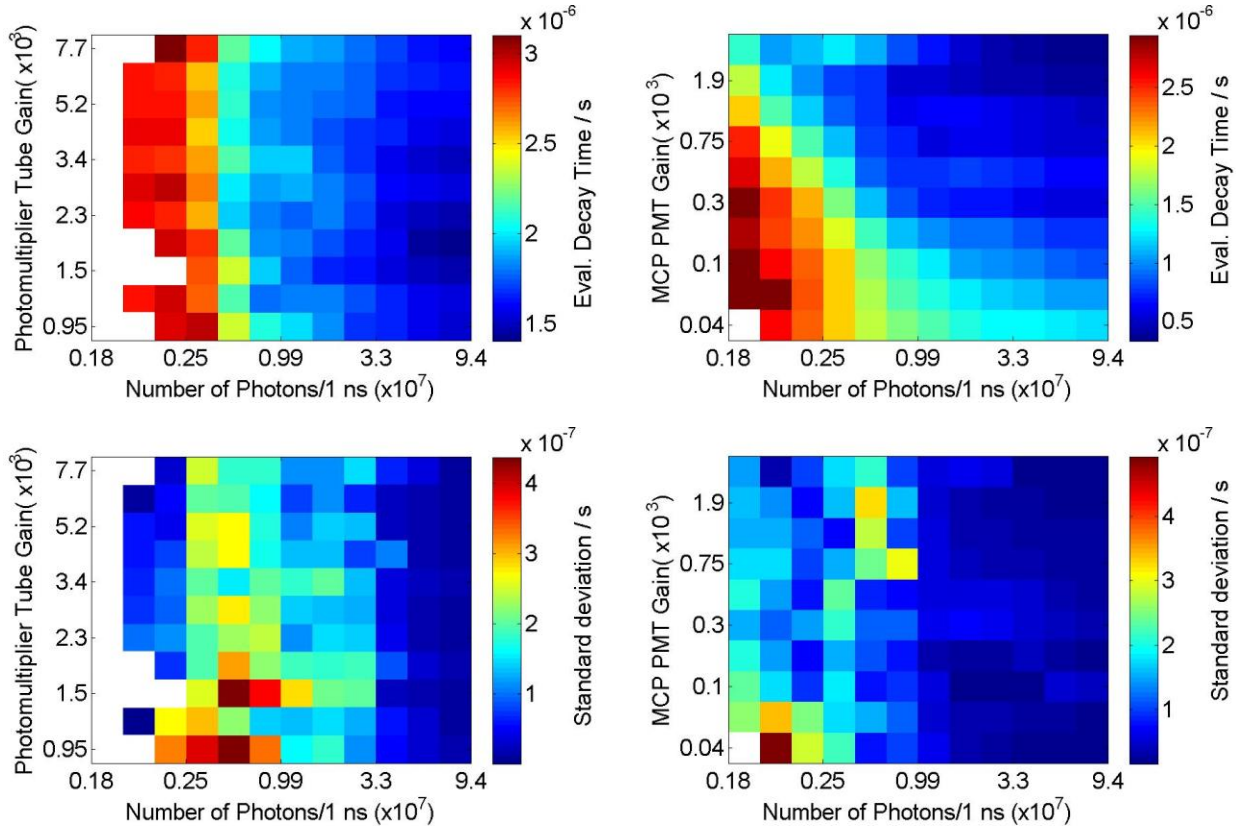

Figure 5.10: Decay time vs. detector gain and number of incident photons at a measurement temperature of 100 °C. *Left:* time-gated PMT time-gated mode decay time and standard deviation (below), *right:* MCP-PMT time-gated mode decay time and standard deviation (below).

The linearity pattern of the time-gated PMT indicated that obtaining linear response is achieved more easily compared to the MCP-PMT. This is because for the time-gated PMT, linearity can be achieved after reaching phosphorescence intensity higher than a certain peak value. In the case of the MCP-PMT, both phosphorescence intensity and gain affect the linearity of the device.

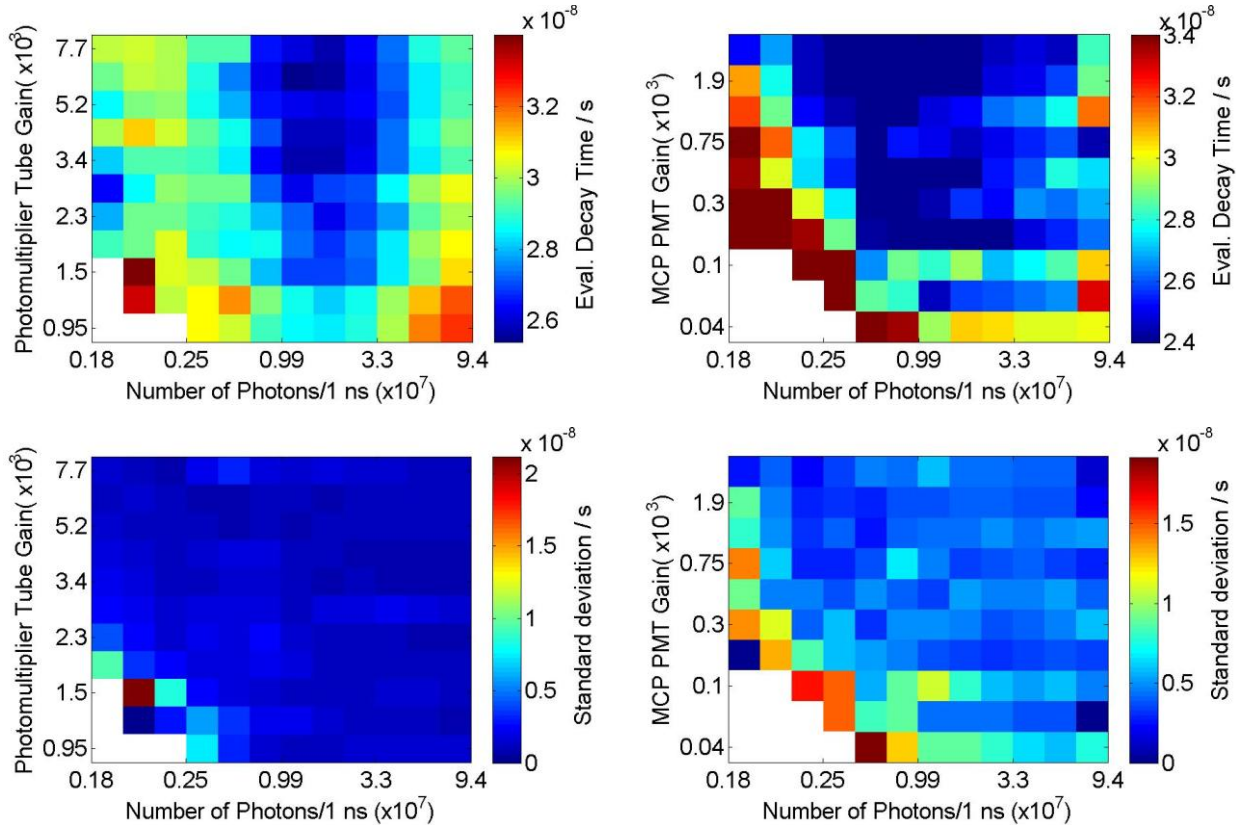

Figure 5.11: Decay time vs. detector gain and number of incident photons at a measurement temperature of 246 °C. *Left:* time-gated PMT time-gated mode decay time and standard deviation (below), *right:* MCP-PMT time-gated mode decay time and standard deviation (below).

Figure 5.11 indicates that the time-gated PMT and the MCP-PMT have lost cells of linear behavior due to low phosphorescence intensity. The region of linear response is centered at almost the same location for both of the detectors, at a region of medium gain and medium to high input intensity levels. At high temperatures, the time-gated PMT and the MCP-PMT provide almost similar linear properties. Due to the limitations of the time-gate width of the MCP-PMT, the time gated PMT provides superior flexibility in decay time measurement condition.

6. Conclusion and Outlook

Response matrices for four detectors were built and regions of linear response were located. Matrices were produced at five temperatures that were set to cover the decay time range of the $CdWO_4$ phosphor. Fixed window evaluation routine for the computation of the decay time is used. Fixed window parameters were chosen for each temperature and applier similarly for each detector. The detectors were used in different modes of operation, which permitted further comparison between the effects of different modes of operation. The normal PMT showed linear response regions in areas of high light intensity and low gain. Saturation was detected at high phosphorescence input levels and at high gain. However, connecting the PMT through a current to voltage amplifier extends the linearity response of the PMT. This extension is brought by using the PMT at low gain values and using the amplification supplier by the amplifier to compensate. The result is a peak signal that has the same registered intensity as that taken by normal PMT mode, but with a linear response in relation to the evaluated decay time. The amplifier introduces a broadening to the amplified signal, but this effect can be eliminated by implementing an amplifier with high bandwidth. The time-gated PMT reveals to be the most promising device tested in this measurement. It was capable of delivering a linear response similar to that of the amplified mode of operation of the normal PMT. Furthermore, the time gated PMT has the ability to run under two different modes of operation. The first mode is continuous which means that PMT is in normal mode. The second available mod is the time-gated mode that has a time gate width that extends from 100ns up to DC. Time gating PMT would prove more effective if applied to phosphors that are characterized by an intense peak just before the exponential phosphorescence decay. The MCP-PMT provides a linearity response that is the inverse of that provided by normal PMT. In other words, the MCP-PMT region of linear operation is located at cells with high input phosphorescence intensity and high gain. The limited width of the MCP-PMT renders the device useless in the detection of decay times that exceed 1 μs. The APD reverse voltage was changed and a response matrix has been built, but the Si-APD fails to provide a gain range that competes with the rest of the detectors. Operating the APD near the breakdown voltage proved to cause nonlinearity in the evaluated decay time.

These measurements are vital to show the decay time drift for each detector. In laser-induced phosphorescence, the accuracy and precision of the determination of the decay times plays an important role in the validity of the data. For this reason, this study aimed to clarify the effects of detector nonlinearity on the deviation of the evaluated decay time and consequently the temperature. This overview provided by the detector specific response matrix, grants a deeper investigation that takes the detector gain and input light intensity as factors.

The time-gated PMT is the most promising detector with large area of linear response in relation to the detection of laser induced phosphorescence signals emitted from $CdWO_4$. The efficiency of time gating could be further studied by employing a phosphor that is characterized by an intense peak compared to the phosphorescence decay. The elimination of the intense peak using time-gated PMT makes it possible to increase the gain and thus improve the signal to noise ratio of the phosphorescence decay.

Further study of the low phosphorescence intensity decay time gradient should be done to determine the causes of this behavior. Since in engine measurements the measured signal is quite week due to soot and other particles absorption, it is critical to investigate the effect of the decay time gradient on measured temperatures. Solution or compensation methods could be concluded to help minimize the resulting deviation in evaluated temperature.

References

1. Childs, P.R.N., J.R. Greenwood, and C.A. Long, *Review of temperature measurement.* Review of Scientific Instruments, 2000. 71(8): p. 2959-2978.
2. Khalid, A. and K. Kontis, *Thermographic Phosphors for High Temperature Measurements: Principles, Current State of the Art and Recent Applications.* Sensors, 2008. 8(9): p. 5673-5744.
3. Allison, S.W. and G.T. Gillies, *Remote thermometry with thermographic phosphors: Instrumentation and applications.* Review of Scientific Instruments, 1997. 68(7): p. 2615-2650.
4. Heyes, A.L., S. Seefeldt, and J.P. Feist, *Two-colour phosphor thermometry for surface temperature measurement.* Optics & Laser Technology. 38(4-6): p. 257-265.
5. Feist JP, H.A., Seefeldt S, *Thermographic phosphors for gas turbines: instrumentation development and measurement uncertainties.* 11th International symposium on Application of Laser Techniques to Fluid Mechanics, Lisbon, Portugal,, 2002.
6. Särner, G., *Laser-Induced Emission Techniques for Concentration and Temperature Probing in Combustion*, in *Division of Combustion Physics*. 2008, Lund University: Lund.
7. Abraham, Y., N.A.W. Holzwarth, and R.T. Williams, *Electronic structure and optical properties of CdMoO_{4} and CdWO_{4}.* Physical Review B, 2000. 62(3): p. 1733-1741.
8. Rzhevskaya, O., et al., *Optical and luminescence properties of CdWO(4) and CdWO(4):Mo single crystals.* Optics and Spectroscopy, 2008. 104(3): p. 366-373.
9. Kobayashi, M., et al., *Cadmium tungstate scintillators with excellent radiation hardness and low background.* Nuclear Instruments and Methods in Physics Research Section A: Accelerators, Spectrometers, Detectors and Associated Equipment, 1994. 349(2-3): p. 407-411.
10. Shevchuk, V.N. and I.V. Kayun, *Dipole effects in luminescent crystals.* Radiation Measurements. 42(4-5): p. 847-850.
11. Chirila, M.M., et al., *Photoluminescence study of cadmium tungstate crystals.* Journal of Physics and Chemistry of Solids, 2000. 61(5): p. 675-681.
12. Saint-Gobain, *Cadmium Tungstate Scintillation Material*, S.-G.C.P. Inc, Editor. 2005.
13. Sharman, K.K., et al., *Error Analysis of the Rapid Lifetime Determination Method for Double-Exponential Decays and New Windowing Schemes.* Analytical Chemistry, 1999. 71(5): p. 947-952.
14. Ballew, R.M. and J.N. Demas, *Error analysis of the rapid lifetime determination method for single exponential decays with a non-zero baseline.* Analytica Chimica Acta, 1991. 245(0): p. 121-127.
15. Ballew, R.M. and J.N. Demas, *An error analysis of the rapid lifetime determination method for the evaluation of single exponential decays.* Analytical Chemistry, 1989. 61(1): p. 30-33.
16. Photonics, H., *Photomultiplier Tubes Construction and Operating Characteristics.* 1998: Japan.
17. Photonis, *Photomultiplier tubes basics*, Photonis, Editor. 2002.
18. Photonics, H., *Photomultiplier Tubes: Basics and Applications.* 2006.
19. Photonics, H., *Characteristics and use of Si APD (Avalanche Photodiode)*, H. Photonics, Editor. 2004. p. 12.
20. Photonics, H., *Photodiode technical information*, H. Photonics, Editor.

21. Wood, J.C.S., *Establishing and Maintaining System Linearity*, in *Current Protocols in Cytometry*. 2001, John Wiley & Sons, Inc.
22. Lee, H.S., et al., *Gated photomultiplier response characterization for DIAL measurements.* Applied Optics, 1990. 29(22): p. 3303-3315.
23. Bristow, M.P., *Lidar-Signal Compression by Photomultiplier Gain Modulation: Influence of Detector Nonlinearity.* Appl. Opt., 1998. 37(27): p. 6468-6479.
24. Fenster, A., et al., *Linearity and Fatigue in Photomultipliers.* Review of Scientific Instruments, 1973. 44(6): p. 689-694.
25. Lush, H.J., *Photomultiplier linearity.* Journal of Scientific Instruments, 1965. 42(8): p. 597.
26. Bristow, M.P., D.H. Bundy, and A.G. Wright, *Signal linearity, gain stability, and gating in photomultipliers: application to differential absorption lidars.* Applied Optics, 1995. 34(21): p. 4437-4452.
27. Knappe, C., et al., *Response Regime Studies on Standard Detectors for Decay Time Determination in Phosphor Thermometry.* Proceedings of the 9th International Temperature Symposium, 2012.
28. Quantel, *Pulsed Nd:YAG lasers*, Quantel, Editor.
29. Brübach, J., J.P. Feist, and A. Dreizler, *Characterization of manganese-activated magnesium fluorogermanate with regards to thermographic phosphor thermometry.* Measurement Science and Technology, 2008. 19(2): p. 025602.